Using the climate feedback response method to quantify climate feedbacks in the middle atmosphere in WACCM

Maartje Sanne Kuilman[1], Qiong Zhang[2], Ming Cai[3], Qin Wen[1,4]

1. Department of Meteorology and Bolin Centre for Climate Research, Stockholm University, Stockholm, Sweden
2. Department of Physical Geography and Bolin Centre for Climate Research, Stockholm University, Stockholm, Sweden
3. Department of Earth, Ocean and Atmospheric Science, Florida State University, Tallahassee, Florida, USA
4. Laboratory for Climate and Ocean-Atmosphere Studies (LaCOAS), Department of Atmospheric and Oceanic Sciences, School of Physics, Peking University, Beijing, China

Corresponding author: Maartje Sanne Kuilman (maartje.kuilman@misu.su.se)

Abstract

Over recent decades it has become clear that the middle atmosphere has a significant impact on surface and tropospheric climate. A better understanding of the middle atmosphere and how it reacts to the current increase of the concentration of carbon dioxide (CO_2) is therefore necessary. In this study, we investigate the response to a doubling CO_2 in the middle atmosphere using the Whole Atmosphere Community Climate Model (WACCM). We use the climate feedback response analysis method (CFRAM) to calculate the partial temperature changes due to an external forcing and climate feedbacks in the atmosphere. As this method has the unique feature of additivity, these partial temperature changes are linearly addable. In this study, we discuss the direct forcing of CO_2 and the effects of the ozone, water vapour, cloud, albedo and dynamical feedbacks.

As expected, our results show that the direct forcing of CO_2 cools the middle atmosphere. This cooling becomes stronger with increasing height: the cooling in the upper stratosphere is about three times as strong as the cooling in the lower stratosphere. The ozone feedback yields a radiative feedback that mitigates this cooling in most regions of the middle atmosphere. However, in the tropical lower stratosphere and in some regions of the mesosphere, the ozone feedback has a cooling effect. The increase in CO_2-concentration causes the dynamics to change. The temperature response due to this dynamical feedback is small in the global average, although there are large temperature changes due to this feedback locally. The temperature change in the lower stratosphere is influenced by the water vapour feedback and to a lesser degree by the cloud and albedo feedback. These feedbacks play no role in the upper stratosphere and the mesosphere. We find that the effects of the changed SSTs on the middle atmosphere are relatively small as compared to the effects of changing the CO_2. However, the changes in SSTs are responsible for dynamical feedbacks that cause large temperature

changes. Moreover, the temperature response to the water vapour feedback in the lower stratosphere is almost solely due to changes in the SSTs. As CFRAM has not been applied to the middle atmosphere in this way before, this study also serves to investigate the applicability as well as the limitations of this method. This work shows that CFRAM is a very powerful tool to study climate feedbacks in the middle atmosphere. However, it should be noted that there is a relatively large error term associated with the current method in the middle atmosphere, which can be for a large part be explained by the linearization in the method.

1. Introduction

The increase of concentration of carbon dioxide in the atmosphere forms a major perturbation to the climate system. It is commonly associated with lower-atmospheric warming. However, in the middle atmosphere, the increase of CO_2 leads to a cooling of the region instead. This cooling has been well documented and is found by both model studies and observations (e.g. *Manabe and Wetherald*, 1975; *Ramaswamy et al.*, 2001; *Beig et al.,* 2003).

The middle atmosphere is not only affected by the increase in CO_2-concentration, but also by the decrease in ozone-concentration. The depletion of ozone (O_3) also effects the temperature in the stratosphere and leads to a cooling (*Shine et al,* 2003). A better understanding of the effect of the increased CO_2-concentration on the middle atmosphere, will help to distinguish the effects of the changes CO_2- and O_3-concentration.

Another major motivation for this study is the emerging evidence that the middle atmosphere has an important influence on surface and tropospheric climate (*Shaw and Shepherd*, 2008). It has, for example, been shown that cold winters in Siberia are linked to changes in the stratospheric circulation (*Zhang et al.*, 2018).

Nowack et al. (2015) has found that there is an increase in global mean surface warming of about 1°C when the ozone is prescribed at pre-industrial levels, as compared with when it is evolving in response to an abrupt 4xCO_2 forcing. It should be noted that the exact importance of changes in ozone seems to be dependent on both the model and the scenario (*Nowack et al.*, 2015) and is not found by all studies (*Marsh et al.*, 2016).

As the effect is found to be rather large in some studies, and absent in other, there is a need for a better understanding of the behaviour of the middle atmosphere in response to changing CO_2 conditions, as the ozone concentration is influenced by this. Ozone is an example of a climate feedback, a process that changes in response to a change in CO_2-concentration and in turn dampens or amplifies the climate response to the CO_2 perturbation.

These climate feedbacks are a challenging subject of study, as observed climate variations might not be in equilibrium, multiple processes are operating at the same time and moreover the geographical structures and

99   timescales of different forcings differ. However, feedbacks form a crucial part
100   of understanding the response of the atmosphere to changes in the CO_2-
101   concentration.

102   Various methods have been developed to study these feedbacks, such as the
103   partial radiative perturbation (PRP) method, the online feedback suppression
104   approach and the radiative kernel method (*Bony et al.,* 2006 and the
105   references therein). These methods study the origin of the global climate
106   sensitivity (*Soden and Held*, 2006; *Caldwell et al.*, 2016; *Rieger et al*., 2017).
107   The focus of these methods is on changes in the global mean surface
108   temperature, global mean surface heat and global mean sensible heat fluxes
109   (*Ramaswamy et al., 2019*).

110   These methods are powerful for this purpose; however, they are not suitable
111   to explain temperature changes on spatially limited domains. They neglect
112   non-radiative interactions between feedback processes and they only account
113   for feedbacks that directly affect the radiation at the top of the atmosphere
114   (TOA).

115   The climate feedback-response analysis method (CFRAM) is an alternative
116   method which takes into account that the climate change is not only
117   determined by the energy balance at the top of the atmosphere, but is also
118   influenced by the energy flow within the Earth's system itself (*Cai and Lu,*
119   *2009, Lu and Cai*, 2009). The method is based on the energy balance in an
120   atmosphere-surface column. It solves the linearized infrared radiation transfer
121   model for the individual energy flux perturbations. This makes it possible to
122   calculate the partial temperature changes due to an external forcing and these
123   internal feedbacks in the atmosphere. It has the unique feature of additivity,
124   such that these partial temperature changes are linearly addable.
125
126   As a practical diagnostic tool to analyse the role of various forcing and
127   feedback, CFRAM has been used widely in climate change research on
128   studying surface climate change (*Taylor et al.,* 2013; *Song and Zhang,* 2014;
129   *Hu et al.,* 2017; *Zheng et al.,* 2019). CFRAM has been applied to study the
130   middle atmosphere climate sensitivity as well (*Zhu et al.,* 2016). In their study,
131   Zhu et al. *(2016)* have adapted CFRAM and applied it to both model output,
132   as well as observations. The atmospheric responses during solar maximum
133   and minimum were studied and it was found that the variation in solar flux
134   forms the largest radiative component of the middle atmosphere temperature
135   response.
136
137   In the present work, we apply CFRAM to climate sensitivity experiments
138   performed with the Whole Atmosphere Community Climate Model (WACCM),
139   which is a high-top global climate system model, including the full middle
140   atmosphere chemistry.
141
142   We investigate the middle atmosphere response to CO_2-doubling. We
143   acknowledge that such idealized equilibrium simulation cannot reproduce the
144   complexity of the atmosphere, in which the CO_2-concentration is changing

145 gradually. However, simulating a double CO_2-scenario still allows us to
146 identify robust feedback processes in the middle atmosphere.
147
148 There are two aspects of the middle atmosphere response to CO_2-doubling:
149 there is the effect of the changes in CO_2-concentration directly, as well as the
150 changes in sea surface temperature (SST) which are in itself caused by the
151 changes in CO_2-concentration. It is useful to investigate these aspects
152 separately, as former should be robust, while the effect of the changed SST
153 depends on the changes in tropospheric climate, which can be expected to
154 depend more on the model.
155
156 In this study, we investigate the effects of doubling the CO_2-concentration and
157 the accompanying sea surface temperature change on the temperature in the
158 middle atmosphere as compared to the pre-industrial state. We use CFRAM
159 to calculate the radiative contribution to the temperature change due to
160 changes in carbon dioxide directly as well as due to changes in ozone, water
161 vapour, albedo, and clouds. We refer to the changes in ozone, water vapour,
162 albedo and clouds in response to changes in the CO_2-concentration as the
163 ozone, water vapour, albedo and cloud feedbacks.
164
165 The circulation in the middle atmosphere is driven by waves. Wave forcing
166 drives the temperatures in the middle atmosphere far away from radiative
167 equilibrium. In the mesosphere, there is a zonal forcing, which yields a
168 summer to winter transport. In the polar winter stratosphere, there is a strong
169 forcing that consists of rising motion in the tropics, poleward flow in the
170 stratosphere and sinking motion in the middle and high latitudes. This
171 circulation is referred to as the 'Brewer-Dobson circulation' (*Brewer,* 1949;
172 *Dobson*, 1956).

173 Dynamical effects make important contributions to the middle-atmosphere
174 energy budget, both through eddy heat flux divergence and through adiabatic
175 heating due to vertical motions. It is therefore important that we also consider
176 changes to the middle-atmosphere climate due to dynamics. We refer to this
177 as the 'dynamical feedback' (*Zhu et al*., 2016).

178 The main goal of this paper is to calculate the contribution to the temperature
179 change due to changes in carbon dioxide directly as well as due to changes in
180 ozone, water vapour, albedo, clouds and dynamics in the middle atmosphere
181 under a double CO_2-scenario using CFRAM. Our intention is not to give a
182 complete account of the exact mechanisms behind the changes in ozone,
183 water vapour, albedo, clouds and dynamics.

184 **2. The model and methods**
185
186 **2.1 Model description**

187 The Whole Atmosphere Community Model (WACCM) is a chemistry-climate
188 model, which spans the range of altitudes from the Earth's surface to about
189 140 km (*Marsh et al.,* 2013). The model consists of 66 vertical levels with
190 irregular vertical resolution, which ranges from ~1.1 km in the troposphere,

191 1.1–1.4 km in the lower stratosphere, 1.75 km at the stratosphere and 3.5 km
192 above 65 km. The horizontal resolution is 1.9° latitude by 2.5° longitude.

193 WACCM is a superset of the Community Atmospheric Model version 4
194 (CAM4) developed at the National Center for Atmospheric Research (NCAR).
195 Therefore, WACCM includes all the physical parameterizations of CAM4
196 (*Neale et al.,* 2013), and a well-resolved high-top middle atmosphere. The
197 orographic gravity wave (GW) parameterization is based on *McFarlane*
198 (1987). WACCM also includes parameterized non-orographic GWs, which are
199 generated by frontal systems and convection (*Richter et al.,* 2010). The
200 parameterization of non-orographic GW propagation is based on the
201 formulation by *Lindzen* (1981).

202 The chemistry in WACCM is based on version 3 of the Model for Ozone and
203 Related Chemical Tracers (MOZART3). This model represents chemical and
204 physical processes from the troposphere until the lower thermosphere.
205 (*Kinnison et al.,* 2007). In addition, WACCM simulates chemical heating,
206 molecular diffusion and ionization and gravity wave drag.

2.2 Experimental set-up

208 In this study, the F_1850 compset (component set) of the model is used, i.e.
209 the model assumes pre-industrial (PI) conditions. This compset simulates an
210 equilibrium state, which means that it runs a perpetual year 1850. Four
211 experiments have been performed for this study (see Table 1).

212 Experiment C1 is the control run, with the pre-industrial CO_2 concentration
213 (280 ppm) and forced with pre-industrial ocean surface conditions such as
214 sea surface temperature and sea ice (referred to SSTs from now on). These
215 SSTs are generated from the CMIP5 pre-industrial control simulation by the
216 fully coupled Earth system model CESM. The atmospheric component of
217 CESM is the same as WACCM, but does not include stratospheric chemistry
218 (*Hurrell et al.,* 2013). This latter aspect is not considered in this study.

219 Experiment C2 represents the experiment with the CO_2 concentration doubled
220 as compared to the pre-industrial state (560 ppm) and forced with the same
221 pre-industrial SSTs as in experiment C1. In WACCM, the CO_2-concentration
222 does not double everywhere in the atmosphere. Only the surface level CO_2
223 mixing ratio is doubled, and elsewhere in the atmosphere is calculated
224 according to WACCM's chemical model.

225 The compset used in this experiment and all the following ones is still F_1850,
226 which means that other radiatively and chemically active gases, such as
227 ozone, will change only because of the changes in the CO_2-concentration,
228 due to WACCM's interactive chemistry. Chlorofluorocarbons (CFCs), which
229 have a major impact on the ozone concentration in the real atmosphere, don't
230 play a role in our experiments.

231 In experiment S1, we simulate the scenario, in which there is the SSTs forcing
232 from the coupled CESM for double CO_2 condition, but the pre-industrial CO_2-

233 concentration of 280 ppm. S2 represents the experiment with the CO_2-
234 concentration in the atmosphere doubled to 560 ppm and the SSTs
235 prescribed for the double CO_2-climate. Experiment C1, C2, S1 and S2 will be
236 also referred to hereafter by PI, the simulation with high CO2, the simulation
237 with high SSTs and the simulation with high CO_2 and SSTs, respectively.

238 The experimental setup of this study is similar to the setup performed with the
239 Canadian Middle Atmosphere Model (CMAM) *by Fomichev et al.* (*2007*) and
240 with the Hamburg Model of the Neutral and Ionized Atmosphere
241 (HAMMONIA) by *Schmidt et al.* (2006). The HAMMONIA model is coupled to
242 the same chemical model as WACCM: MOZART3. The setup in their study is
243 similar, however, in their study, they double the CO_2-concentration from 360
244 ppm to 720 ppm, while in our study, we double from the pre-industrial level of
245 CO_2 (280 ppm).

246 Note that experiment S1 and C2 are not representing scenarios that could
247 happen in the real atmosphere. These experiments have been used to study
248 the effect of the SSTs separately. Experiment S2 doesn't take into account
249 other (anthropogenic) changes in the atmosphere not caused by changes in
250 the CO_2-concentration and the SSTs.

251 All the simulations are run for 50 years, of which the last 40 years are used for
252 analysis. In the all results shown, we have used the 40 year mean of our
253 model data.

254 Table 1. Set-up of the model experiments.

Experiment	CO_2	SSTs from CESM equilibrium run
C1	280 ppm	PI control
C2	560 ppm	PI control
S1	280 ppm	Double CO_2 run
S2	560 ppm	Double CO_2 run

255 **2.3 Climate feedback-response analysis method (CFRAM)**

256 In this study, we aim to quantify the different climate feedbacks that may play
257 a role in the middle atmosphere in a double CO_2-climate. For this purpose, we
258 apply the climate feedback-response analysis method (CFRAM) (*Lu and Cai*,
259 2009).
260
261 As briefly discussed in the introduction, traditional methods to study climate
262 feedbacks are based on the energy balance at the top of the atmosphere
263 (TOA). This means that the only climate feedbacks that are taken into
264 consideration are those that effect the radiative balance at the TOA. However,
265 there are other thermodynamic and dynamical processes that do not directly
266 affect the TOA energy balance, while they do yield a temperature response in
267 the atmosphere.
268
269 Contrary to TOA-based methods, CFRAM considers all the radiative and non-
270 radiative feedbacks that result from the climate system due to response to an

271 external forcing. This means that CFRAM starts from a slightly different
272 definition of a feedback process. Note also that as the changes in temperature
273 are calculated simultaneously, the vertical mean temperature or lapse rate
274 feedback per definition do not exist in CFRAM.
275
276 Another advantage of CFRAM is that it allows for measuring the magnitude of
277 a certain feedback in units of temperature. We can actually calculate how
278 much of the temperature change is due to which process. The *'climate*
279 *response'* in the name of this method refers to the changes in temperature in
280 response to the climate forcings and climate feedbacks.
281
282 We refer to the Appendix for the complete formulation of CFRAM diagnostics
283 using outputs of WACCM. Based on the linear decomposition principle, we
284 can solve Eq. (A12) for each of the terms on its right-hand side. This yields
285 the partial temperature changes due to each specific process namely:
286

287 $$\Delta T_{CO_2} = \left(\frac{\partial \vec{R}}{\partial \vec{T}}\right)^{-1} \Delta(\vec{S} - \vec{R})_{CO_2} \qquad (1)$$

288

289 $$\Delta T_{O_3} = \left(\frac{\partial \vec{R}}{\partial \vec{T}}\right)^{-1} \Delta(\vec{S} - \vec{R})_{O_3} \qquad (2)$$

290

291 $$\Delta T_{H_2O} = \left(\frac{\partial \vec{R}}{\partial \vec{T}}\right)^{-1} \Delta(\vec{S} - \vec{R})_{H_2O} \qquad (3)$$

292

293 $$\Delta T_{albedo} = \left(\frac{\partial \vec{R}}{\partial \vec{T}}\right)^{-1} \Delta(\vec{S} - \vec{R})_{albedo} \qquad (4)$$

294

295 $$\Delta T_{cloud} = \left(\frac{\partial \vec{R}}{\partial \vec{T}}\right)^{-1} \Delta(\vec{S} - \vec{R})_{cloud} \qquad (5)$$

296

297 The factors $\Delta(\vec{S} - \vec{R})_{CO_2}$, $\Delta(\vec{S} - \vec{R})_{O_3}$, $\Delta(\vec{S} - \vec{R})_{H_2O}$, $\Delta(\vec{S} - \vec{R})_{albedo}$ and

298 $\Delta(\vec{S} - \vec{R})_{cloud}$ are calculated by inserting the output variables from WACCM in
299 the radiation code of CFRAM. Here, one takes the output variables from the
300 control run, apart from the variable that is related to the direct forcing or the
301 feedback.
302
303 This means that for the direct forcing of CO_2, one takes the CO_2 from the
304 perturbation run, while one takes the other variables from the control run. For
305 the ozone feedback, one takes the ozone from the perturbation run. For the
306 water vapour feedback, one takes the specific humidity, surface pressure,
307 surface temperature and dew point temperature. While for the albedo
308 feedback, one takes the downwelling solar flux at surface and net solar flux at
309 surface from the perturbation run and the other variables from the control run.
310 For the cloud feedback, one takes the cloud fraction, cloud ice and cloud
311 liquid amount from the perturbation run. For all these feedbacks, one takes
312 the other variables from the control run.
313

314   Similarly, to equations (1)-(5), we also calculate the temperature change due
315   to non-LTE processes and the dynamical feedback. We calculate the terms
316    $\Delta(\vec{S} - \vec{R})_{non-LTE}$ and Δdyn in Eq. (A4) and (A7).
317

318    $$\Delta T_{non-LTE} = \left(\frac{\partial \vec{R}}{\partial \vec{T}}\right)^{-1} \Delta(\vec{S} - \vec{R})_{non-LTE} \qquad (6)$$

319    $$\Delta T_{dyn} = \left(\frac{\partial \vec{R}}{\partial \vec{T}}\right)^{-1} \Delta dyn \qquad (7)$$

320
321   The calculated partial temperature changes can be added, their sum being
322   equal to the total temperature change. It is important to note that this does not
323   mean that the individual processes are physically independent of each other.
324

325    $$\Delta T_{CFRAM} = + \Delta T_{O_3} + \Delta T_{H_2O} + \Delta T_{albedo} + \Delta T_{cloud} + \Delta T_{non-LTE} + \Delta T_{dyn}$$
326    $$(8)$$

327
328   The linearization done for equations (A9) and (A10) introduces an error
329   between the temperature difference as calculated by CFRAM and as seen in
330   the model output. Another source of error is that the radiation code of the
331   CFRAM calculations is not exactly equal to the radiation code of WACCM.
332

333    $$\Delta T_{CFRAM} = \Delta T_{WACCM} - \Delta T_{error} \qquad (9)$$

334
335   For more details on the CFRAM method, please refer to *Lu and Cai* (2009).
336

337   Note that the method used in this study differs from the Middle Atmosphere
338   Climate Feedback Response Analysis Method (MCFRAM) used by *Zhu et al.*
339   (2016). The major difference is that in this study, we perform the calculations
340   using the units of energy fluxes (Wm^{-2}) instead of converting to heating rates
341   (Ks^{-1}). In other words, we use Wm^{-2} as the units of heating rates for the layer
342   between two adjacent vertical levels. Because the radiative heating rates are
343   the net radiative energy fluxes entering the layer, it is rather natural and
344   straightforward (i.e., without dividing the mass in the layer to convert it to units
345   of Ks^{-1}) to have the same units of heating rates (convergence) as the radiative
346   energy fluxes. Another difference is that our method is not applicable above
347   0.01 hPa (~80 km), while *Zhu et al.* (2016) added molecular thermal
348   conduction to the energy equation, to perform the calculations beyond the
349   mesopause.
350

351   **3. Temperature responses in a double CO_2 scenario**
352

353   As described in section 2.2, four experiments were performed with WACCM: a
354   simulation with pre-industrial conditions (experiment C1) , a simulation with
355   changed SSTs only (experiment S1), a simulation with only a changed CO_2-
356   concentration (experiment C2) and a final simulation with both changed SSTs
357   and CO_2-concentration (experiment S2).
358

359   Figure 1 shows the zonal mean temperature changes for the different
360   experiments with respect to the pre-industrial state, as modelled by WACCM.
361   The results reach a statistical significance of 95% for the whole middle

atmosphere domain in the experiments S2-C1 and C2-C1, and most of the middle atmosphere for experiment S1-C1. For this figure, as well as for all the results shown in this paper, we have used the 40 year mean of our data.

In line with what was shown in earlier studies (e.g. *Akmaev*, 2006; *Fomichev et al.*, 2007), we observe that an increase in CO_2 causes a cooling in the middle atmosphere with the exception of the cold summer upper mesosphere region. We also observe that changing the SSTs alone, while leaving the CO_2-concentration at the pre-industrial levels (Fig 1c and 1f) also yields significant temperature changes over a large part of the middle atmosphere and contributes to the observed warming in the cold summer mesopause region.

As found previously by *Fomichev et al.* (2007) and *Schmidt et al.* (2006), we find that the sum of the two separate temperature changes in the experiment with changed CO_2 only and changed SSTs only (experiment C2 and S1) is approximately equal to the changes observed in the combined simulation (experiment S2). *Shepherd* (2008) has explained this phenomenon as follows: climate change affects the middle atmosphere in two ways: either radiatively through in situ changes associated with changes in CO_2 or dynamically through changes in stratospheric wave forcing, which are primarily a result of changing the SSTs (*Shepherd*, 2008). Even though the radiative and dynamic processes are not independent, these processes are seen to be approximately additive (*Sigmond et al.*, 2004, *Schmidt et al.*, 2006, *Fomichev et al.*, 2007).
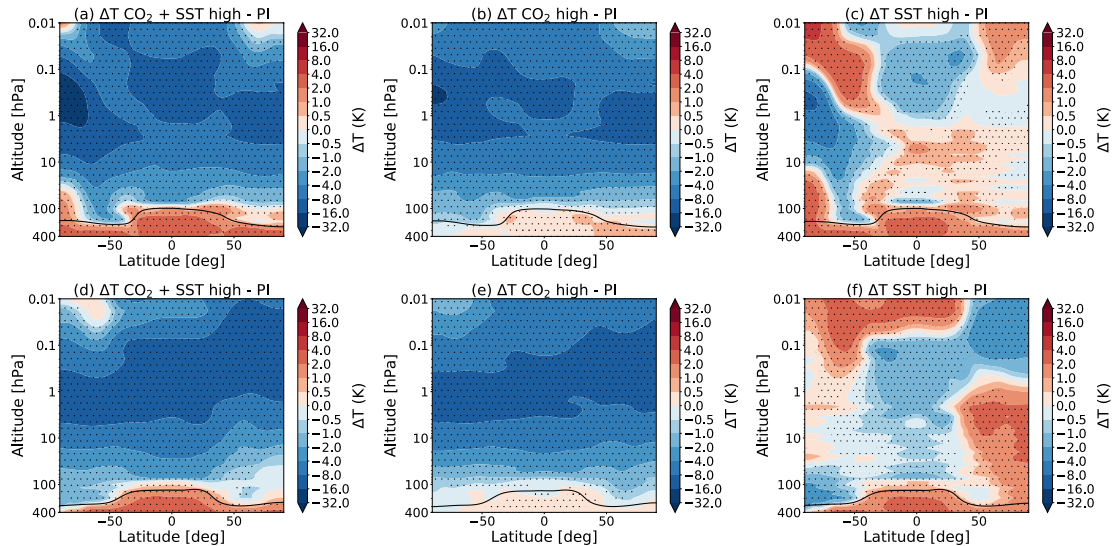
Figure 1: The total change in temperature in July (top) and January (bottom) for (a,d) the simulation with high CO_2 and SSTs, (b,e) the simulation with high CO_2, (c,f) the simulation with high SSTs, all as compared the pre-industrial control simulation. The dotted regions indicate the regions where the data reaches a confidence level of 95%. The black line indicates the tropopause height for the experiments S2 (a,d), C2 (b,e) and S1 (c,f).

4. Meridional-vertical profiles of partial temperature changes

The CFRAM makes it possible to separate and estimate the temperature responses due to an external forcing and various climate feedbacks, such as ozone, water vapour, cloud, albedo and dynamical feedbacks. Note that for the ozone, water vapour, cloud and albedo feedback, we can only calculate the radiative part of the feedback. The response to dynamical changes is calculated in a separate term.

This can be understood as we use the Fu-Liou radiative transfer model (*Fu and Liou,* 1992, 1993) to do offline calculations of the total local thermal equilibrium (LTE) radiative heating rate perturbation fields between the control experiment C1 and one of the other three experiments (i.e, C2, or S1, or S2). We use the standard outputs of atmospheric compositions (e.g., CO_2 and O_3) and thermodynamic fields (e.g., pressure, temperature, water vapour, clouds, surface albedo) as well as partial LTE radiative heating rate perturbation fields due to perturbations in individual atmospheric composition or thermodynamic fields (e.g., the terms on the right hand side of (A.9) except the first term).

We use the difference between the offline calculation of the total LTE radiative heating rate perturbations and the original total LTE radiative heating rate perturbations derived directly from the standard WACCM outputs as the error term of our offline LTE radiative heating perturbations. We note that the standard WACCM output fields also include non-LTE radiative heating fields, but do not include non-radiative heating rates. Therefore, we use the sum of the total LTE radiative heating rate perturbations and non-LTE radiative heating fields derived from the standard WACCM output fields to infer non-radiative heating rate perturbations under the equilibrium condition, namely Eq. (A.8).

We should also note that, because we are using an atmosphere-only model, in our experiment, the external forcing is either the change in CO_2-concentration or the change in SSTs or both. In an atmosphere-ocean model (such as CESM) and, of course, in reality, the changes in sea surface temperature and sea ice distributions are responses to the changed CO_2-concentration.

In this section, we discuss the meridional-vertical profiles of the temperature responses to the direct forcing and the various feedbacks during July and January. In the next section, we will discuss regional and global means of partial temperature changes due to feedbacks.

4.1 Direct temperature response to CO_2

Figure 2 shows the zonal mean temperature change due to the increase in CO_2. We see that increasing CO_2 leads to a cooling almost everywhere in the middle atmosphere, except at the high latitudes in the cold summer upper mesosphere, where we see a warming instead. The higher the temperature, the more cooling due to the increasing CO_2-concentration (*Shepherd,* 2008). The reason for this is that the outgoing longwave radiation strongly depends on the Planck blackbody emission (*Zhu et al.,* 2016).
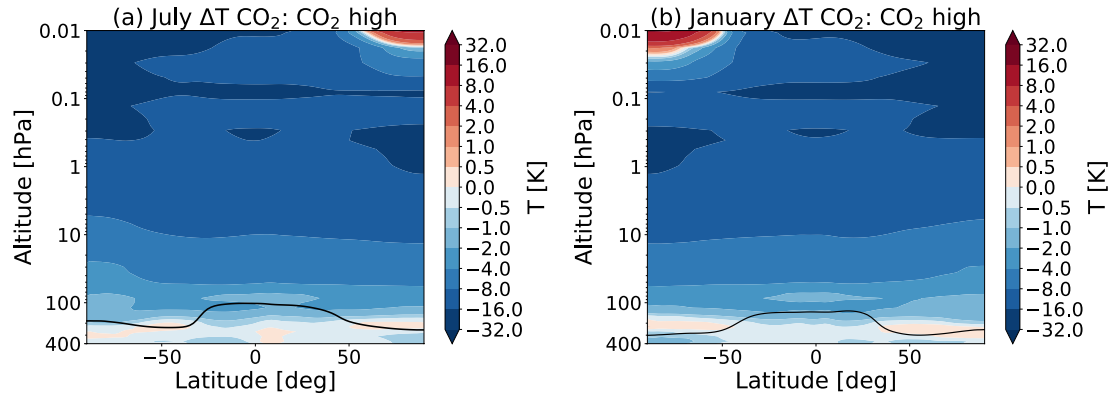
Figure 2: Partial temperature change due to the direct forcing of CO_2 for July (top) and January (bottom) due to the doubling of the atmospheric CO_2-concentration, as calculated by CFRAM, using experiment C2 and C1. The black line indicates the tropopause height for the C2 runs (with double CO_2-concentration).

Changing the SSTs does not lead to a change in CO_2-concentration, therefore the temperature response to changes in CO_2 is not present for the run with only changed SST (Figures not shown).

4.2 Ozone feedback

Ozone plays a crucial role in the chemical and radiative budget of the middle atmosphere. The distribution of ozone in the middle atmosphere is determined by both chemical and dynamical processes. Most of the ozone production takes place in the tropical stratosphere, as a result of photochemical processes, which involve oxygen. Meridional circulation then transports ozone to other parts of the middle atmosphere (*Langematz*, 2019). The production of ozone is largely balanced by catalytic destruction cycles involving NO_x, HO_x and Cl_x radicals. HO_x dominates ozone destruction in the mesosphere and lower stratosphere, while NO_x and Cl_x dominate this process in the middle and upper stratosphere (e.g. *Cariolle*, 1983).

Since the 1970s ozone in the middle atmosphere began to decline globally, due to increased production of ozone depleting substances (ODSs) (*Brühl and Crutzen*, 1988). The Montreal Protocol, adopted in 1987 to stop this threat, eventually led to a slow recovery of the stratospheric ozone over the recent two decades (*WMO*, 2018; *Langematz*, 2019). In our study, we don't consider the effect of anthropogenic ODSs since pre-industrial times (*Langematz*, 2019).

In this study, we are interested in the temperature response to changes in ozone concentration induced by the increased CO_2 concentration and/or the changes in SST in WACCM. Under enhanced CO_2 concentrations, the ratio between O_3 and O mixing ratios is generally shifted toward a higher concentration of ozone, which is caused by the strong temperature dependency of the ozone production reaction ($O + O_2 + M \rightarrow O_3 + M$).

482   Fig. 3 shows the percentage changes in O_3-concentration when the CO_2-
483   concentration and/or the SSTs change. The results reach a statistical
484   significance of 95% for the whole middle atmosphere domain in the
485   experiments S2-C1 and C2-C1, and most of the middle atmosphere for
486   experiment S1-C1.
487
488   We find, as expected, that an increase in CO_2, leads to an increase of ozone
489   in most of the middle atmosphere. The increase of O_3 is about 20% around 2
490   hPa in the tropical region for experiment S2 with respect to C1. This
491   corresponds with what is seen by *Fomichev et al., (2007),* however they find
492   that the increase in ozone in January is a bit lower in this region (around 15%,
493   see their Figure 7).
494
495   There are some regions where the O_3-concentration is decreasing. In the
496   tropical lower stratosphere, a decrease of about 20% is seen, in the summer
497   polar mesosphere (around 0.01 hPa) ozone decreases by 3%, while in the
498   mesosphere (around 0.02 hPa), ozone decreases by over 30%. Fig. 3c and f
499   show that changing the SSTs also has a significant impact on the ozone
500   concentration. A complete account of the ozone changes is out of the scope
501   of this paper.
502
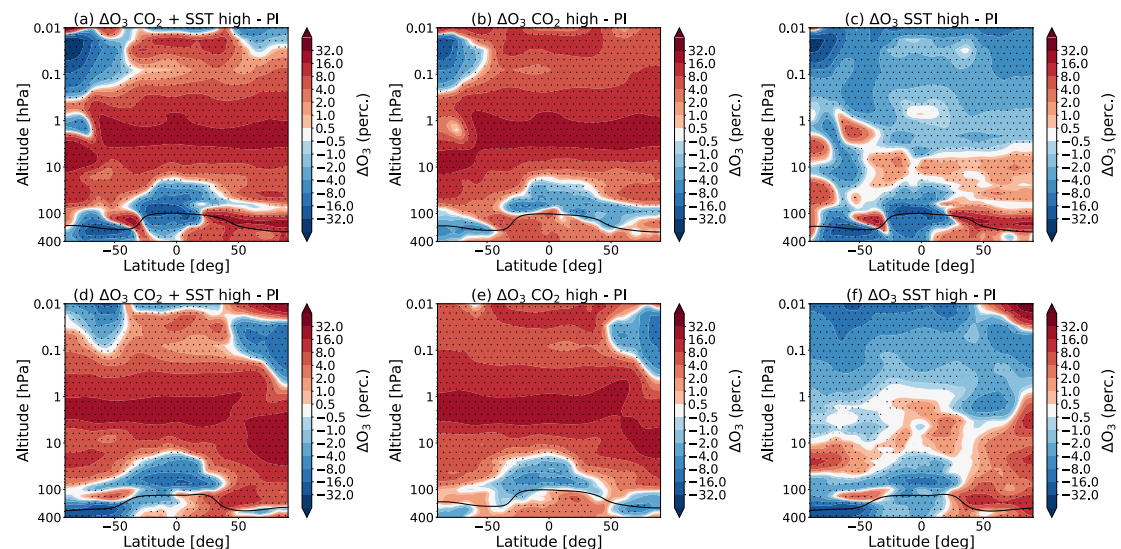
503
504 Figure 3: The percentage change in the zonal and monthly mean ozone
505 concentration for July (top) and January (bottom) due to (a,d) combined effect
506 of the CO_2 increase and SSTs changes (experiments S2 -C1), (b,e) the
507 doubling of the atmospheric CO_2-concentration (experiments C2 - C1) and the
508 (c,f) SSTs (experiments S1 - C1), as simulated by WACCM. The dotted
509 regions indicate the regions where the data reaches a confidence level of
510 95%. The tropopause height is indicated as in Fig. 1.

511   As we will discuss in the next section, an enhanced concentration of CO_2 also
512   leads to changes in the dynamics in the middle atmosphere. The stratospheric
513   Brewer-Dobson circulation is projected to strengthen, which would lead to an
514   increase in the poleward transport of ozone. We will also see that an increase
515   in CO_2-concentration leads to stronger summer pole-to-winter pole flow in the
516   mesosphere.

517 Figure 4 shows the percentage change in the zonal and monthly mean
518 concentration of Cl, NO, O, OH, CH_3, NO_x and N_2O in July due to combined
519 effect of the CO_2 increase and SSTs changes (experiment S2 vs C1), as
520 simulated by WACCM. The patterns in January look similar (not shown).
521 These results reach a statistical significance of 95% for the whole middle
522 atmosphere domain.

523 We would like to point out that the changes in these constituents are only
524 brought about by the CO_2-concentration and/or the SSTs. We still use the
525 F_1850 compset and the only difference between the runs is the forcing in
526 CO_2 and SSTs. The changes in chemical constituents look very similar to
527 those found by *Schmidt et al.* (2006) who performed a similar experiment as
528 discussed in section 2.2, see their Figure 20. Note that Fig. 4 shows the
529 changes due to both the CO_2 increase and SSTs changes, while their Figure
530 20 shows the percentage changes due the changes in CO_2-concentration only
531 and also only above 1 hPa.

532 As in *Schmidt et al.* (2006), we see an decrease in atomic oxygen (O) mixing
533 ratio at high summer latitudes around 0.01 hPa (see Fig. 4c), which results
534 from increased upwelling. This increase in O leads to a decrease in ozone in
535 this region. We also see decrease of ozone concentration in the winter polar
536 region around 0.1 hPa (approximately 65 km). This could be caused an
537 increase of NO and for a small part by Cl mixing ratios, which result from a
538 stronger subsidence of NO and Cl rich air, as suggested in Schmidt et al.
539 *2006*. As stated before, complete discussion of the changes in ozone
540 concentration is out of the scope of this paper and the changes in other
541 constituents shown in Figure 4 are shown for reference only.

542
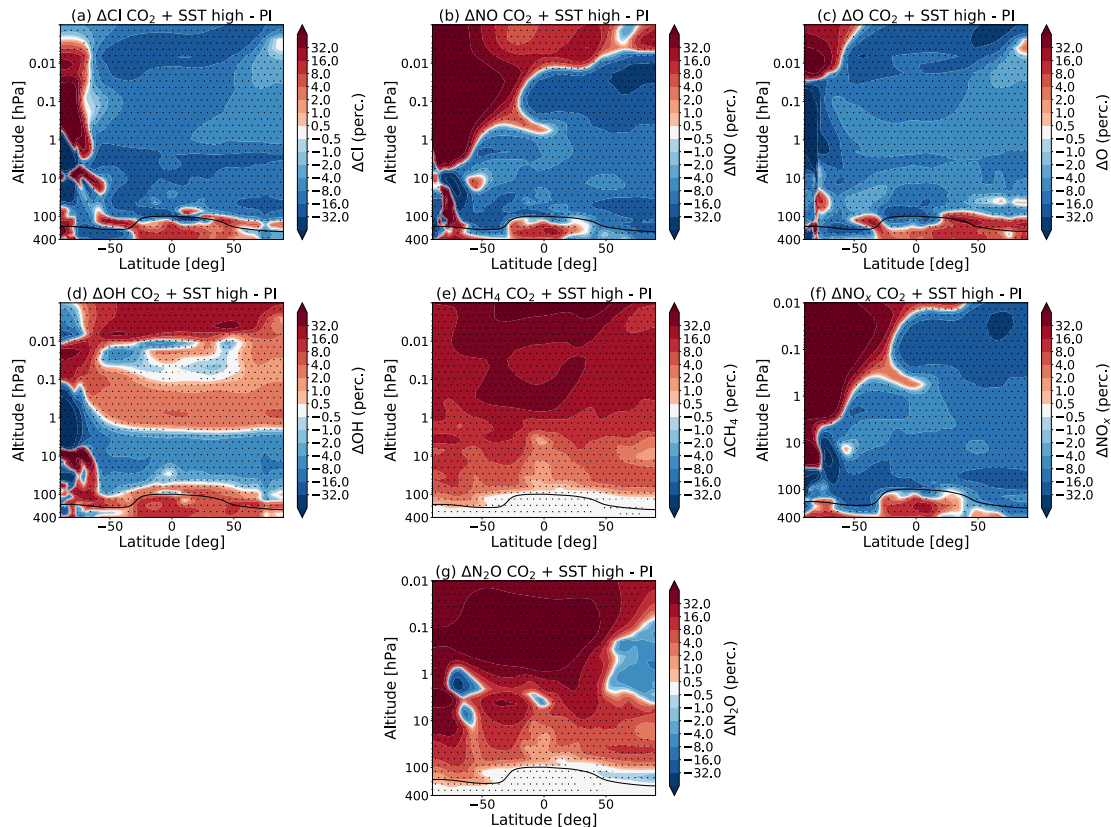
Figure 4: The percentage change in the zonal and monthly mean concentration of Cl (a), NO (b), O (c), OH (d), CH_4 (e) and NO_x (f) and N_2O (g) in July due to combined effect of the CO_2 increase and SSTs changes (experiment (S2 vs C1), as simulated by WACCM. The dotted regions indicate the regions where the data reaches a confidence level of 95%. The tropopause height is indicated as in Fig. 1.

What is new in this study, is that we can calculate the temperature responses due to the changes in ozone concentration. These temperature responses are shown in Figure 5. It can be seen that there is a warming in the regions where there is an increase of the O_3-concentration, while there is a cooling for the regions with a decrease of the O_3-concentration. However, this is not the case for the winter polar region, where there is no sunlight. Note that the temperature responses to the changes in CO_2- and O_3- concentration behave differently in this respect: the temperature responses due to the direct forcing of CO_2 follow the temperature distribution quite closely, while the temperature responses due to O_3 follow the ozone concentration, as also seen by Zhu et al., *(2016).*
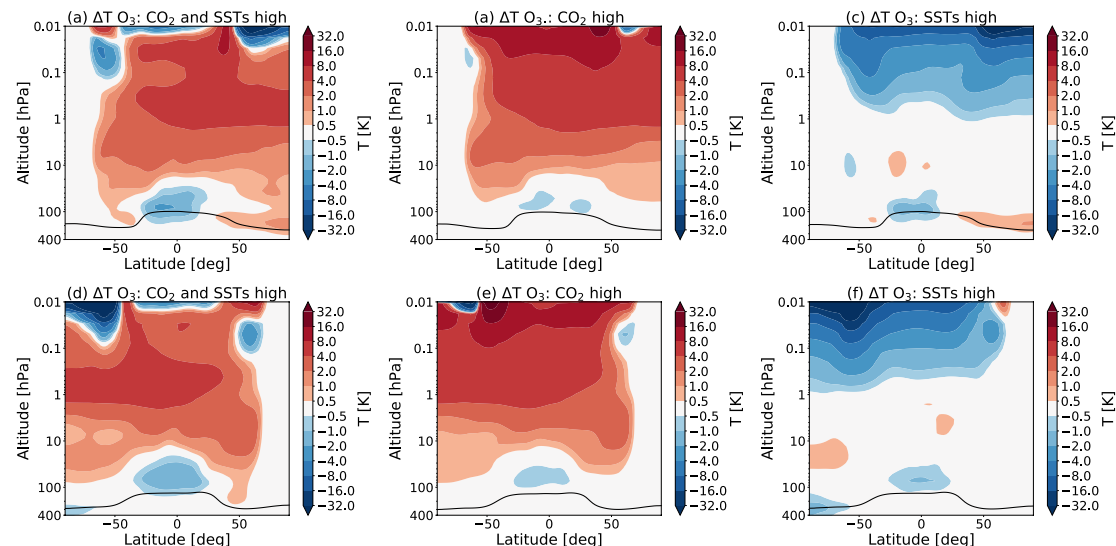
Figure 5: Partial temperature responses to changes in O_3-concentration, as calculated by CFRAM, in July (top) and January (bottom) due to the (a,d) combined effect of the CO_2 increase and SSTs changes (S1), (b,e) the doubling of the atmospheric CO_2-concentration (experiments C2) and the (c,f) SSTs (experiments S1). The tropopause height is indicated as in Fig. 1.

4.2 Dynamical feedback

The zonal mean residual circulation forms an important component of the mass transport by the Brewer-Dobson circulation (BDC). It consists of a meridional ($\overline{v}^*$) and a vertical ($\overline{w}^*$) component as defined in the Transformed Eulerian Mean (TEM) framework. The residual circulation consists of a shallow branch which controls the transport of air in the tropical lower stratosphere, as well as a deep branch in the mid-latitude upper stratosphere and mesosphere.

577 Both of these branches are driven by atmospheric waves. In the winter
578 hemisphere, planetary Rossby waves propagate upwards into the
579 stratosphere, where they break and deposit their momentum on the zonal
580 mean flow, which in turns induces a meridional circulation. The two-cell
581 structure in the lower stratosphere, which is present all-year round, is driven
582 by synoptic scale waves. The circulation is also affected by orographic gravity
583 wave drag in the stratosphere and by non-orographic gravity wave drag in the
584 upper mesosphere (*Oberländer et al*., 2013).

585 Most climate models show that the BDC and the upwelling in the equatorial
586 region will speed up due to an increase in CO_2-concentration (*Butchart el al.,*
587 *2010*). It has been shown that the strengthening of the Brewer-Dobson
588 circulation in the lower stratosphere is caused by changes in transient
589 planetary and synoptic waves, while the upper stratospheric changes are due
590 to changes in the propagation properties for gravity waves (*Oberländer et al*.,
591 2013).

592 It has been explained that the increased stratospheric resolved wave drag is
593 caused by an increase of the meridional temperature gradient in the
594 stratosphere, which leads to a strengthening of the upper flank of the
595 subtropical jets. This in turn shifts the critical layers for Rossby wave breaking
596 upward, which allows for more Rossby waves to reach the lower stratosphere,
597 where they break and deposit their momentum, enhancing the BDC
598 (*Shepherd and McLandress*, 2011)

599 The differences in the meridional component of the residual circulation ($\bar{v}^*$)
600 between the different simulations are shown in Fig. 6. These data are
601 averaged over the 40 years of data. The results reach a statistical
602 significance of 95% almost the whole area above 1 hPa for the experiments
603 C2-C1, for the experiment S1-C1 the results reach a statistical significance of
604 95% in most of the area below this level. The experiments S2-C1 show the
605 largest region of statistical significance, apart from some regions below 1 hPa.

606 Figure 6b and 6e show that only doubling the CO_2 leads to a stronger pole-to-
607 pole flow in the mesosphere. Changing the SSTs also leads to changes in the
608 residual circulation as can be seen in Fig. 6c and 6f. Oberländer et al. (*2013*)
609 have shown that the rising CO_2-concentration affects the upper stratospheric
610 layers, while the signals in the lower stratosphere are almost completely due
611 to changes in sea surface temperature.

612 The warmer sea surface temperatures affect the dynamics in the middle
613 atmosphere. It has for example been shown that higher SSTs in the tropics
614 leads to an amplification in deep convection, which enhances the generation
615 of quasi-stationary waves (*Deckert and Dameris, 2008*). Enhanced SSTs lead
616 to an enhanced dissipation of planetary waves, as well as an enhanced
617 dissipation of orographic and non-orographic waves in the upper stratosphere
618 (*Oberländer et al., 2013*).

619
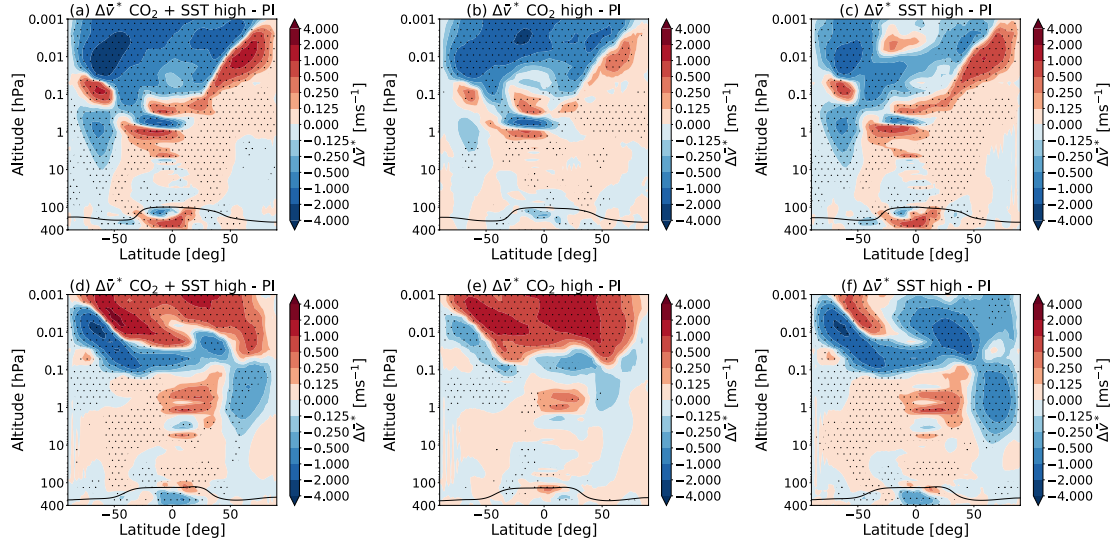
Figure 6: Changes in the zonal and monthly mean transformed Eulerian-mean residual circulation horizontal velocity $\bar{v}^*$ for July (top) and January (bottom) due to (a,d) combined effect of the CO_2 increase and SSTs changes (experiments S2 -C1), (b,e) the doubling of the atmospheric CO_2-concentration (experiments C2 - C1) and the (c,f) SSTs (experiments S1 - C1), as simulated by WACCM. The dotted regions indicate the regions where the data reaches a confidence level of 95%. The tropopause height is as indicated in Fig. 1.

We are interested in the temperature responses due to the dynamical feedbacks in the different experiments. These temperature responses are shown in Figure 7. Figure 7b and 7e show that there is cooling in the summer mesosphere, while there is warming in the winter mesosphere, which is consistent with a stronger summer-to-winter pole flow.

Figure 7c and 7f show the temperature responses due to changes in the SSTs. It is seen that there is mostly a warming in the summer mesosphere and mostly a cooling in the winter hemisphere, which would weaken the effect of the changed CO_2-concentration. Most of the temperature responses in the lower stratosphere are caused by the changes in SSTs, as expected.
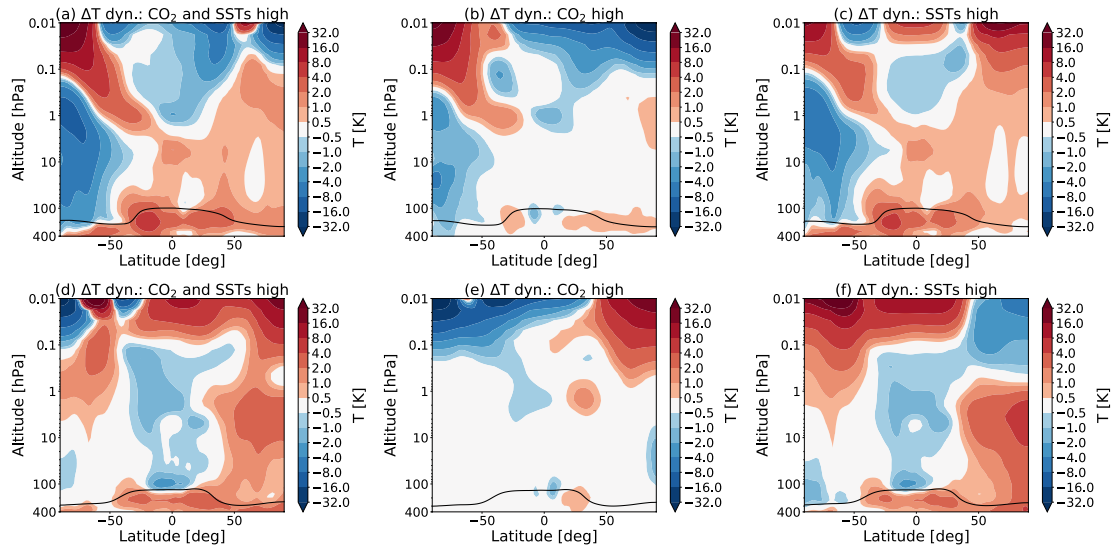
Figure 7: Partial temperature responses to changes in dynamics, as calculated by CFRAM, in July (top) and January (bottom) due to the (a,d) combined effect of the CO_2 increase and SSTs changes (S1), (b,e) the doubling of the atmospheric CO_2-concentration (experiments C2) and the (c,f) SSTs (experiments S1). The tropopause height is indicated as in Fig. 1.

In summary, doubling the CO_2 leads to a stronger pole-to-pole flow in the mesosphere, which leads to cooling of the summer mesosphere and a warming of the winter mesosphere. Changing the SSTs weakens this effect, but leads to temperature changes in the stratosphere and lower mesosphere.

4.4 Water vapour feedback

Figure 8 shows how the water vapour is changing in the middle atmosphere if the CO_2-concentration is increased and/or the SSTs are changed with respect the pre-industrial control run. In WACCM, increasing the CO_2-concentration alone leads to a decrease of water vapour in most of the middle atmosphere (Fig. 8b and f). The results reach a statistical significance of 95% for the whole middle atmosphere domain in the experiments S2-C1 and S1-C1, and most of the middle atmosphere for experiment C2-C1, apart from the winter hemisphere region around 0.1 hPa.

The amount of water vapour in the stratosphere is determined by transport through the tropopause as well as by the oxidation of methane in the stratosphere itself. The transport of the water vapour in the stratosphere is mainly a function of the tropopause temperature (*Solomon et al.,* 2010). In WACCM, we see a decrease in temperature in the tropical tropopause for the double CO_2 experiment of about -0.25 K. The cold temperatures in the tropical tropopause lead to a reduction of water vapour of between 2 and 8% due to freeze-drying in this region.

It can be seen that using the SSTs from the doubled CO_2-climate leads to an increase in water vapour almost everywhere in the middle atmosphere as compared to PI (Fig. 8c and f). In WACCM, forcing with SSTs from a double

672 CO$_2$-climate is observed to lead to a higher and warmer tropopause, which
673 can explain this increase of water vapour. However, it should be noted that
674 models currently have a limited representation of the processes determining
675 the distribution and variability of lower stratospheric water vapour. Minimum
676 tropopause temperatures are not consistently reproduced by climate models
677 (*Solomon et al.,* 2010; *Riese et al.,* 2012). At the same time, observations are
678 not completely clear about whether there is a persistent positive correlation
679 between the SST and the stratospheric water vapour (*Solomon et al.*, 2010).
680
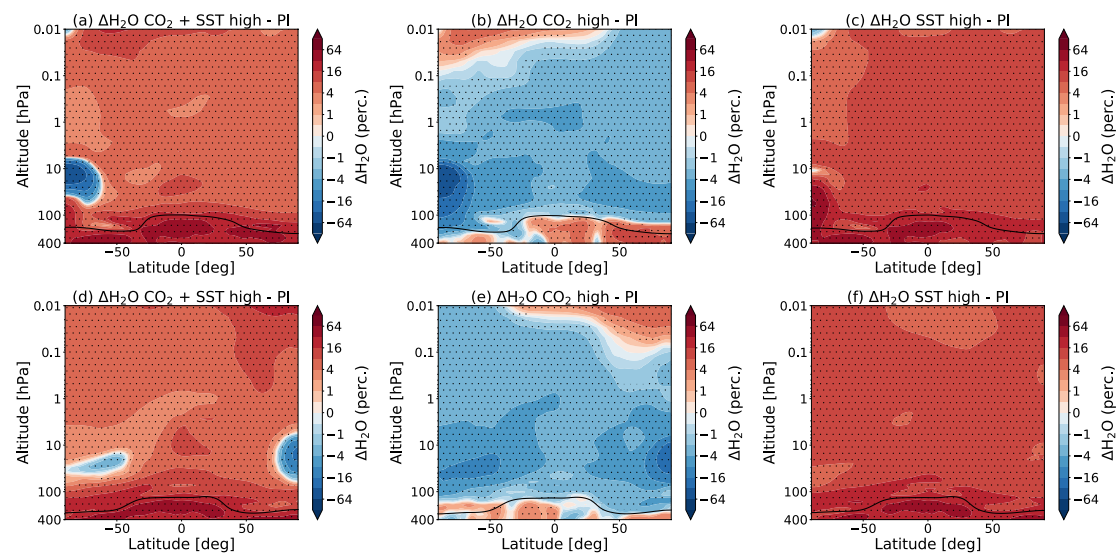
681
682 Figure 8: The percentage changes in the zonal and monthly mean water
683 vapour mixing ratio for July (top) and January (bottom) due to (a,d) combined
684 effect of the CO$_2$ increase and SSTs changes (experiments S2 -C1), (b,e) the
685 doubling of the atmospheric CO$_2$-concentration (experiments C2 - C1) and the
686 (c,f) SSTs (experiments S1 - C1), as simulated by WACCM. The dotted
687 regions indicate the regions where the data reaches a confidence level of
688 95%. The tropopause height is as indicated in Fig. 1.
689
690 Figure 9 shows the temperature responses due to the changes in water
691 vapour as calculated by CFRAM. It can be seen that the regions where there
692 is an increase in the water vapour, there is a cooling, and vice versa. This can
693 be understood as increasing the water vapour in the middle atmosphere leads
694 to an increase in longwave emissions in the mid and far-infrared by water
695 vapour. This in turns leads to a cooling of the region. Similarly, a decrease in
696 water vapour leads to a warming of the region (*Brasseur and Solomon,* 2005).
697 Higher up in the atmosphere, there are large percentage changes in water
698 vapour. However, the absolute concentration of water is small there, which
699 explains why there is no temperature response to these changes.
700
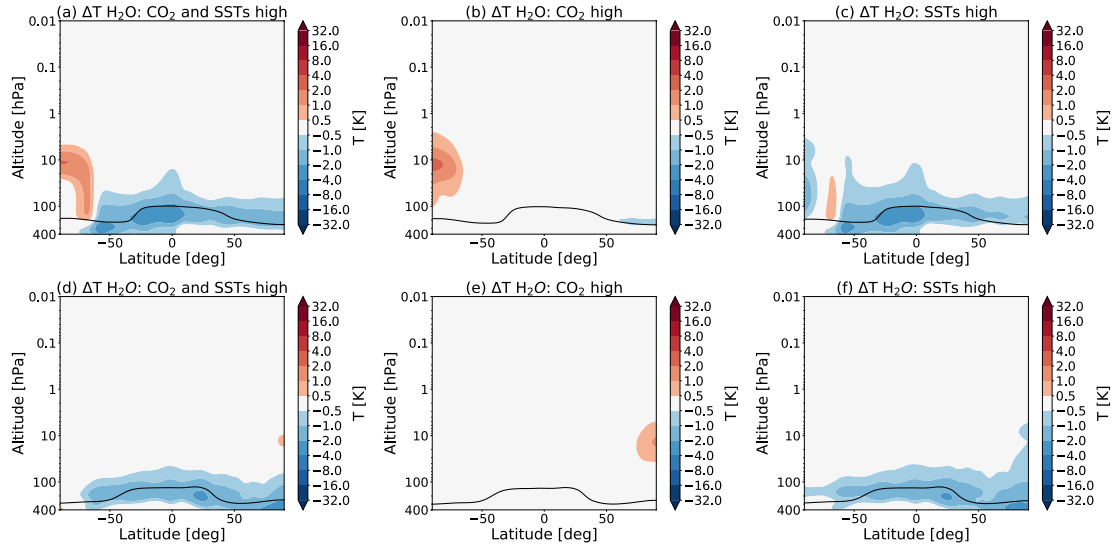
Figure 9: Partial temperature responses to changes in water vapour, as calculated by CFRAM, in July (top) and January (bottom) due to the (a,d) combined effect of the CO_2 increase and SSTs changes (S1), (b,e) the doubling of the atmospheric CO_2-concentration (experiments C2) and the (c,f) SSTs (experiments S1). The tropopause height is indicated as in Fig. 1.

Water vapour plays a secondary but not negligible role in determining the middle atmosphere climate sensitivity. In the lower stratosphere, H_2O contributes considerably to the cooling in this region. Above 30 hPa, the water vapour contribution to the energy budget is negligible, as also seen by *Fomichev et al.* (2007).

4.5 Cloud and albedo feedback

Forcing the model with SSTs from the double CO_2-climate (as in experiment S1 and S2) yields an overall increase in the cloud cover in the upper troposphere, while this is not the case if one only increases the CO_2 concentration (as in experiment C2). Figure 10 shows the temperature responses to changes in cloud (left) and albedo (right) in July (top) and January (bottom) for experiment S1, as calculated by CFRAM.

Fig. 10 shows in the tropical region, there is a warming due to changes in clouds, while there is a cooling at higher latitudes in July (see Figure 10a). In January, the pattern looks slightly different (see Figure 10c). These temperature changes are due to changes in the balance between the increased reflected shortwave radiation and the decrease of outgoing longwave radiation.

We also see an effect of the changes in surface albedo in the stratosphere (see Figure 10b and d). The cooling in the summer polar stratosphere shown in Figure 10b and d is due to radiative changes. We suggest that this cooling is due to a decrease in surface albedo, which would lead to less shortwave radiation being reflected. However, more research is needed.
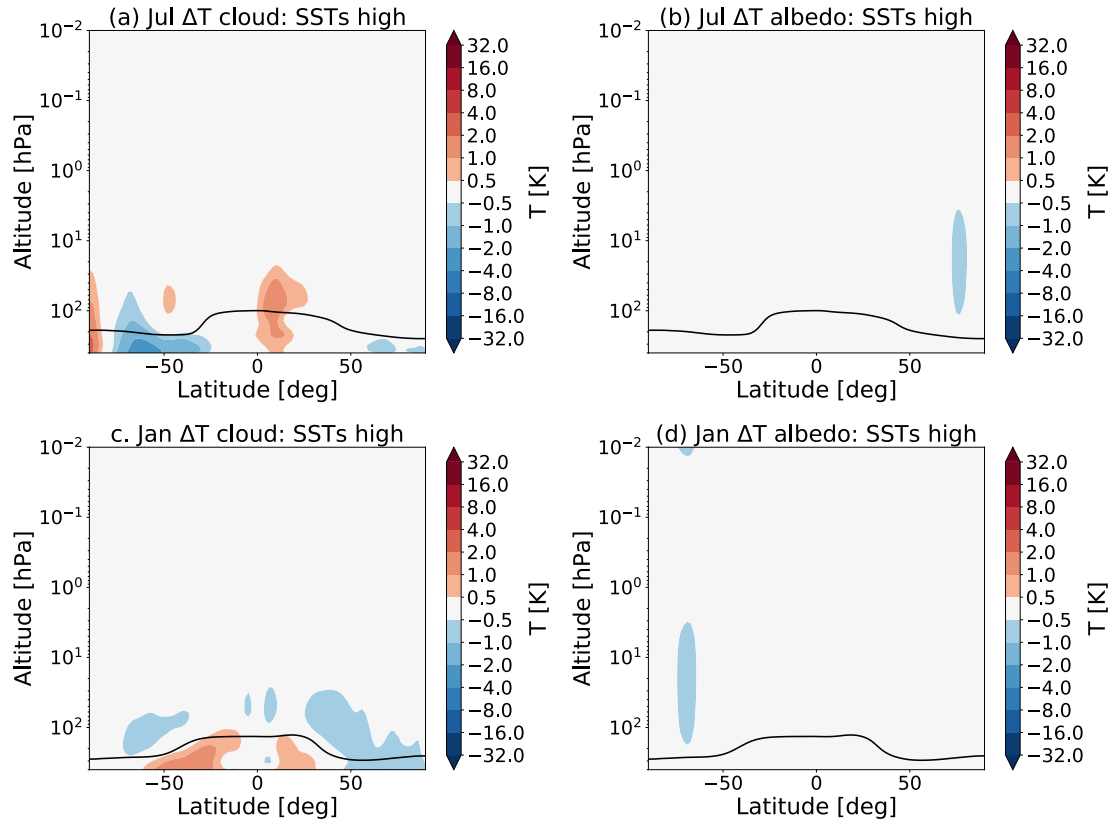
Figure 10: Partial temperature responses to changes in clouds (left) and albedo (right), as calculated by CFRAM, in July (top) and January (bottom) due to the SSTs (experiment S1). The tropopause height is indicated as in Fig. 1.

Cloud and albedo feedbacks due to changes in clouds and surface albedo play a crucial role in determining the tropospheric and surface climate (*Boucher et al.,* 2013, *Royer et al.,* 1990). However, it is clear that these feedbacks play only a very small role in the middle atmosphere temperature response to the doubling of CO_2 and SSTs.

5. Regional and global means of partial temperature changes due to feedbacks

To study the relative importance of the different feedback processes globally we show the average change in global mean temperature for the lower stratosphere, the upper stratosphere and the mesosphere for the S2 experiment with the changed CO_2-concentration and changed SSTs in Figure 11. We also show the average change in temperature in the polar regions (90°S-70°S and 70°N-90°N), the tropics (20°S-20°N) for the lower and upper stratosphere and the mesosphere.

In order to calculate the lower stratosphere temperature changes, we take the average value of the temperature change from the tropopause until 24 hPa. The pressure level of the tropopause is simulated in WACCM for each latitude and longitude, we use this pressure level to demarcate between the troposphere and stratosphere. We consider 24 hPa as a crude estimate for the boundary between the lower and upper stratosphere.

765
766 The tropopause is not exactly at the same pressure level in the perturbation
767 experiments as compared to the pre-industrial control run (C1). We always
768 take the tropopause of the perturbation experiment which is a bit higher at
769 some latitudes, to make sure that we do not use values from the troposphere.
770 We add the values for each latitude up and take the average. This average is
771 not mass weighted. By taking the in this way, we can directly compare the
772 vertical values in different regions of the atmosphere. The temperature
773 changes in the upper stratosphere and in the mesosphere are calculated in
774 the same way, but then for the altitudes 24 hPa-1 hPa and 1 hPa-0.01 hPa
775 respectively.
776
777 Figure 11 shows the radiative feedbacks due to ozone, water vapour, clouds,
778 albedo and the dynamical feedback, as well as the small contribution due to
779 the Non-LTE processes, as calculated by CFRAM. The 'total'-column shows
780 the temperature changes in WACCM, while the column 'error' shows the
781 difference between temperature change in WACCM and the sum of the
782 calculated temperature responses in CFRAM. Note that the range of values
783 on the y-axis is not the same for the different subplots.
784
785 Figure 11 shows that the temperature change in the lower stratosphere due to
786 the direct forcing of CO_2 is around 3 K in the global mean. There is a stronger
787 cooling in the tropical region of about 4 K in July and 3.5 K in January. We
788 also observe that there is a cooling of about 1 K due to ozone feedback in the
789 tropical region while there is a slight warming taking place in the summer
790 hemispheres in both January and July. We also see that the temperature
791 change in the lower stratosphere is influenced by the water vapour feedback.
792 There is a cooling of about 0.5 K in the lower stratosphere, apart from in the
793 southern polar area. There is some small influence from the cloud and albedo
794 feedback, which can be negative or positive (see also Fig. 9).
795
796 In the upper stratosphere, the cooling due to the direct forcing of CO_2 is with
797 about 9 K in the global mean considerably stronger than in the lower
798 stratosphere. The cooling is stronger in the summer polar regions, where the
799 cooling due to the direct forcing of CO_2 reaches 11K. In the winter polar
800 region, this cooling is only about 8K.
801
802 The water vapour, cloud and albedo feedback play no role in the upper
803 stratosphere nor in the mesosphere. The ozone feedback results in the
804 positive partial temperature changes in the upper stratosphere, of about 2 K in
805 the global mean. The changes in ozone don't result in temperature changes in
806 the winter hemisphere, as discussed in section 4.2.
807
808 The picture in the mesosphere is similar as in the upper stratosphere. The
809 main difference is that the temperature changes are larger. The global
810 temperature change due to direct forcing of CO_2 is about 15 K. The O_3-
811 feedback results in a partial temperature changes of about 3 K in the
812 mesosphere in the global mean. The temperature change due to ozone in the
813 equatorial mesosphere is about 4 K, while the warming due to ozone in the

814   summer polar region a bit smaller: around 3K. Just like in the upper
815   stratosphere water vapour, cloud and albedo feedback play no role.
816
817   We see, that the ozone feedback generally yields a radiative feedback that
818   mitigates the cooling, which is due to the direct forcing of CO_2. This has been
819   suggested in earlier studies, such as *Jonsson et al., 2004, Dietmüller et al.,*
820   *2014*. With CFRAM, it is possible to quantify this effect and to compare it with
821   the effects of other feedbacks in the middle atmosphere. Note that no other
822   method before has been able to quantify how much of the temperature
823   change in the middle atmosphere is due to the different feedback processes
824   before.
825
826   The temperature response due to dynamical feedbacks is small in global
827   average: less than 1 K. This can be understood as waves generally do not
828   generate momentum and heat, but redistribute these instead (*Zhu et al.,*
829   2016). However, the local responses to dynamical changes in the high
830   latitudes are large, as we have seen in section 4.2. There are some very small
831   temperature responses due to non-LTE effects as well, which contribute to the
832   temperature change in the mesosphere mostly.
833
834   The error term is relatively large. In CFRAM, we assumed that the radiative
835   perturbations can be linearized by neglecting the higher order terms of each
836   thermodynamic feedback and the interactions between these feedbacks, this
837   yields an error. Cai and Lu (*2009*) show that this error is larger in the middle
838   atmosphere than for similar calculations in the troposphere. In the middle
839   atmosphere, the density of the atmosphere is smaller, which leads to smaller
840   numerical values of the diagonal elements of the Planck feedback matrix. As
841   a result, the linear solution is very sensitive to forcing in the middle
842   atmosphere. Another part of the error is due to the fact that the radiative
843   transfer model used in the offline CFRAM calculations is different than the
844   radiative transfer model used in the climate simulations with WACCM.
845

846
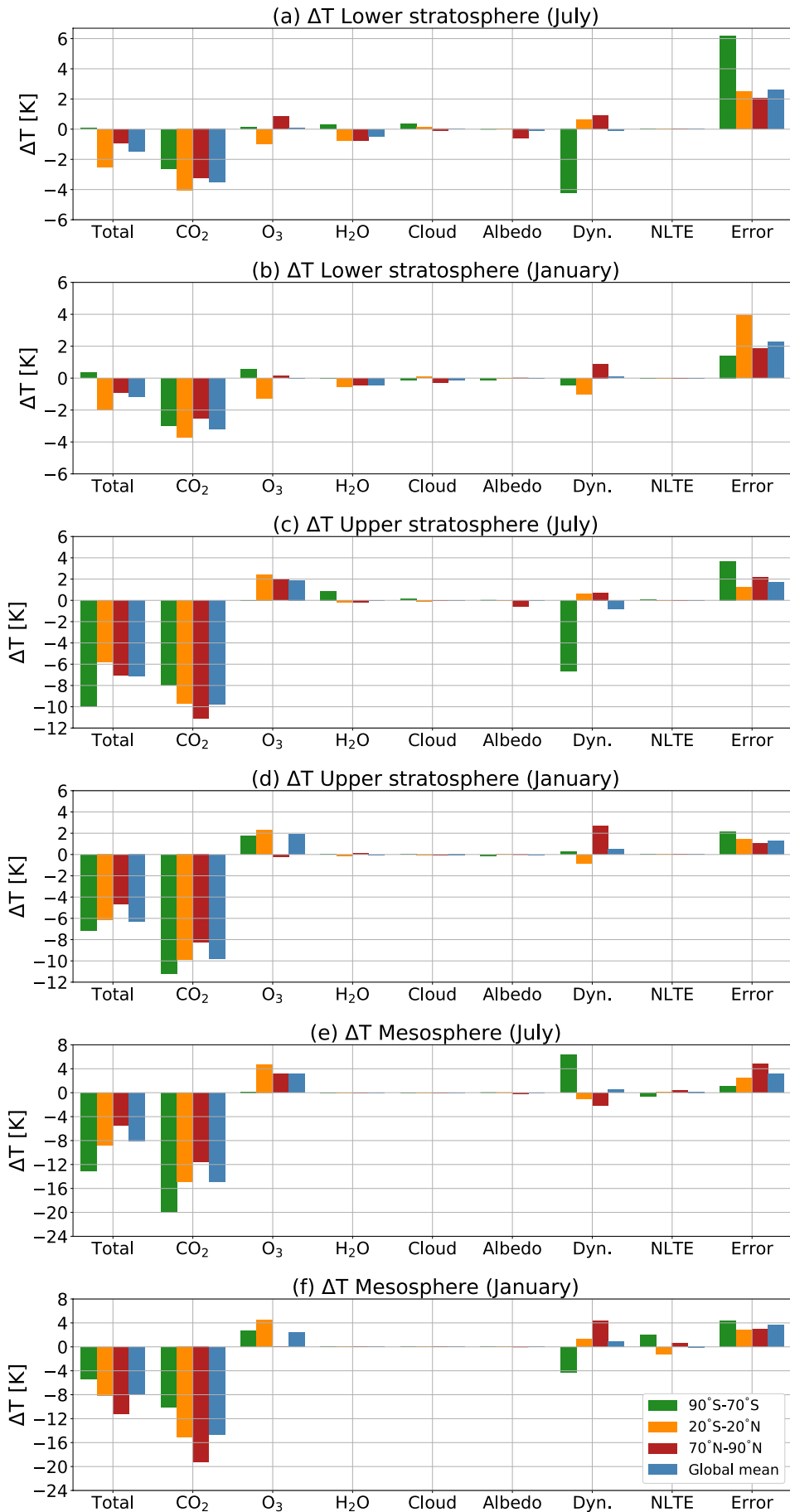
847 Figure 11: The mean temperature responses to the changes in CO_2 and
848 various feedback processes in the lower stratosphere from the tropopause
849 height until 24 hPa (a,b), upper stratosphere from 24-1 hPa (c, d) and in the
850 mesosphere from 1-0.01 hPa (e,f) in July (a, c, e) and January (b, d, f) in the
851 polar regions (90°S-70°S and 70°N-90°N), the tropics (20°S-20°N) and the
852 global mean, for S1 experiment (double CO_2 and changed SSTs). Note that
853 the range of values on the y-axis is not the same for the different subplots.
854
855 In addition, the vertical profiles of the temperature responses to the direct
856 forcing of CO_2 and the feedbacks are shown in Figure 12. Here, one can see
857 that the increase in CO_2 leads to a cooling over almost the whole middle
858 atmosphere; an effect that increases with height. We also observe that in the
859 summer upper mesosphere regions, the increased CO_2-concentration leads
860 to a warming. The changes in ozone concentration in response to the
861 doubling of CO_2 lead to a warming almost everywhere in the atmosphere. In
862 some places, this warming exceeds 5 K. In the polar winter the effect of ozone
863 is small due to lack of sunlight.
864
865 There is also a relatively large temperature response to the changes in
866 dynamics. In Fig. 12, it can be seen that there is a cooling in the summer
867 mesosphere, while there is warming in the winter mesosphere. The water
868 vapour, cloud and albedo feedback play only a very small role in the middle
869 atmosphere, as we observed in Figure 11. The Non-LTE effects are also
870 small, but start to play a small role above 0.1 hPa, the exact mechanism of
871 which is outside the scope of this paper.
872

Temperature responses to different feedback processes
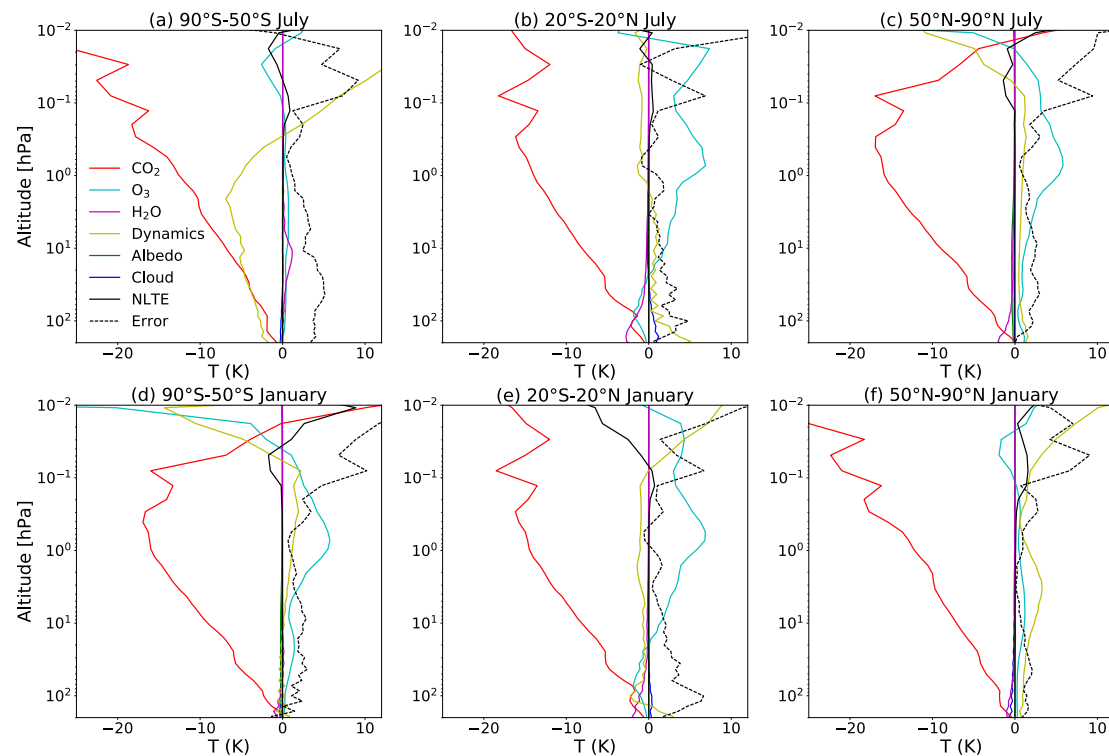
873
874 Figure 12: Vertical profiles of the temperature responses to the changes in
875 CO_2 and various feedback processes in July (top) and January (bottom) for

due to double CO_2 and changed SSTs in the atmosphere between 200 and 0.01 hPa, for regions from 50° N/S poleward and the tropics (20°S-20°N), as calculated by CFRAM.
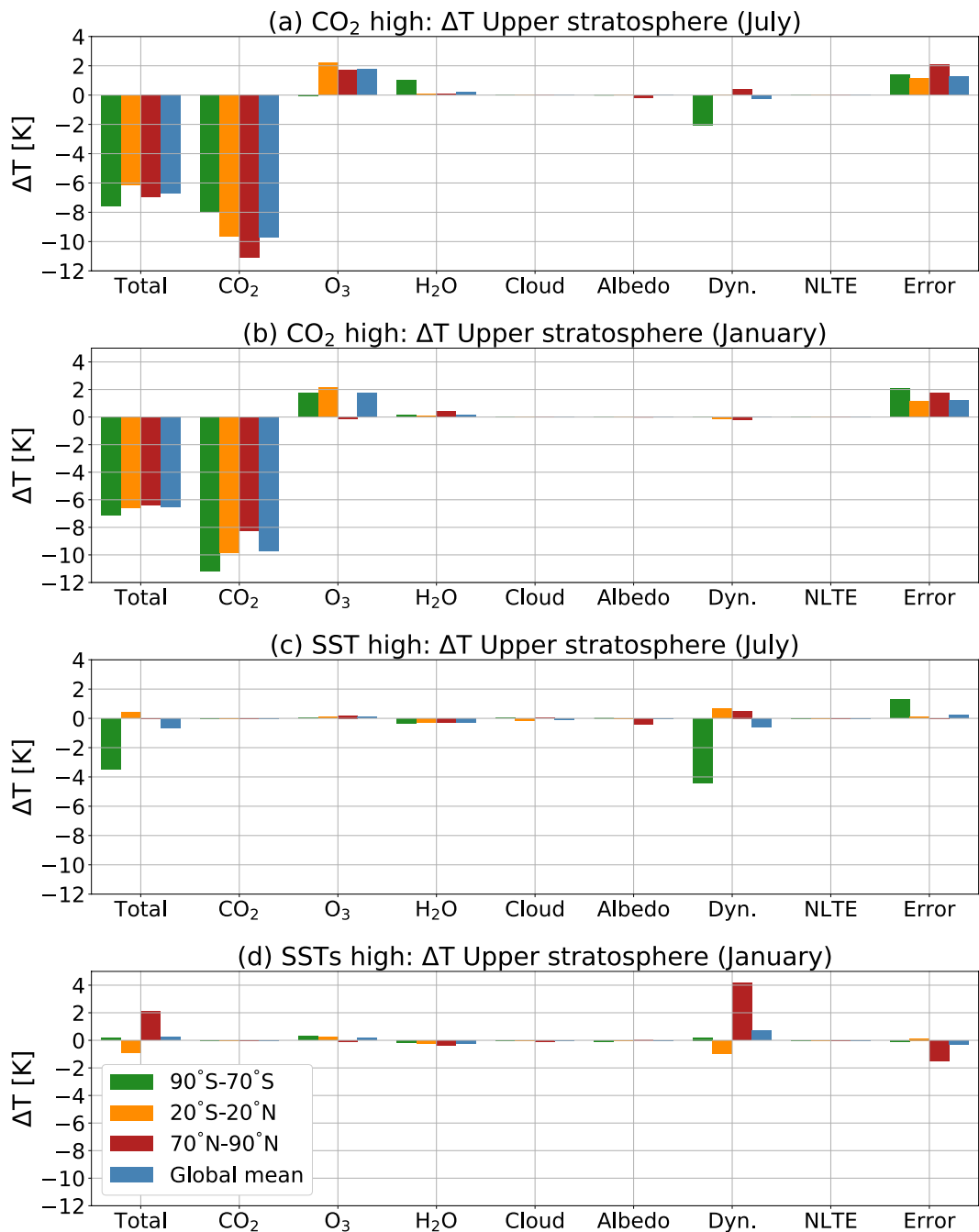
Figure 13: The mean temperature responses to the changes in CO_2 and various feedback processes in July (a,c) and January (b,d) in the upper stratosphere between 24 and 1 hPa, for polar regions (90°S-70°S and 70°N-90°N), the tropics (20°S-20°N) and the global mean for the experiment with double CO_2 (C2) (a,b) and changed SSTs (S1) (c,d) separately.

890 Figure 13 shows temperature responses in the upper stratosphere for the
891 experiment with double CO_2 (a,b) and changed SSTs (c,d) separately. This
892 has been done to give insight in the temperature response of the CO_2 and the
893 SST separately. These temperature changes were calculated in the same
894 way as for Fig. 11. Again also, the 'total'-column shows the temperature
895 changes as simulated by WACCM, the columns CO_2, O_3, H_2O, cloud, albedo,
896 dynamics, Non-LTE shows the temperature responses as calculated by
897 CFRAM. Error shows the difference between temperature change in WACCM
898 and the sum of the calculated temperature responses in CFRAM.

900 We learn from this figure that the effects of the changed SSTs on the upper
901 stratosphere are relatively small as compared to the effects of changing the
902 CO_2. We show the temperature changes for the upper stratosphere as an
903 example. In the lower stratosphere and the mesosphere, we see the same
904 pattern: the effect of the CO_2 on the temperature is generally much larger than
905 the effect of the SSTs on the temperature. This finding is consistent with the
906 study of *Fomichev et al.* (2007), where it is concluded that the impact of
907 changes in SSTs on the middle atmosphere is relatively small and localized
908 as compared to the combined response of changing the CO_2-concentration
909 and the SSTs.

911 The changes in SSTs are, however, responsible for large temperature
912 changes as a result of the dynamical feedbacks, especially in the winter
913 hemispheres, where there is a temperature response of 4K. A similar figure
914 for the lower stratosphere (not shown) shows that the temperature response
915 to the water vapour feedback is almost solely due to changes in the SSTs and
916 not the direct forcing of CO_2.

918 Earlier, we discussed that the sum of the two separate temperature changes
919 in the experiment with double CO_2 and changed SSTs is approximately equal
920 to the changes observed in the combined simulation. We find that the same is
921 true for the temperature responses to the different feedback processes.

923 **5. Discussion and conclusions**

925 In this study, we have applied the climate feedback response analysis method
926 to climate sensitivity experiments performed by WACCM. We have examined
927 the middle atmosphere response to CO_2 doubling with respect to the pre-
928 industrial state. We investigated the combined effect of doubling CO_2 and
929 subsequent warming SSTs, as well as the effects of separately changing the
930 CO_2 and the SSTs. It is important to note that no other method before has
931 been able to quantify how much of the temperature change in the middle
932 atmosphere is due to the different feedback processes before.

934 It was found before that the sum of the two separate temperature changes in
935 the experiment with only changed CO_2 and only changed SSTs is, at first
936 approximation, equal to the changes observed in the combined simulation
937 (see e.g. *Fomichev et al. (2007) and Schmidt et al. (2006)*). This is also the
938 case for WACCM.

939
940 We have found that, even though changing the SSTs yields significant
941 temperature changes over a large part of the middle atmosphere, the effects
942 of the changed SSTs on the middle atmosphere are relatively small as
943 compared to the effects of changing the CO_2 without changes in the SSTs.
944

945 We have given an overview of the mean temperature responses to the
946 changes in CO_2 and various feedback processes in the lower stratosphere,
947 upper stratosphere and in the mesosphere in January and July. We find that
948 the temperature change due to the direct forcing of CO_2 increases with
949 increasing height in the middle atmosphere. The temperature change in the
950 lower stratosphere due to the direct forcing of CO_2 is around 3 K. There is a
951 stronger cooling in the tropical lower stratosphere of about 4 K in July and 3.5
952 K in January.

953 In the upper stratosphere, the cooling due to the direct forcing of CO_2 is about
954 9 K, which is considerably stronger than in the lower stratosphere. The
955 cooling is stronger in the summer polar regions, where the cooling reaches a
956 value of 11K, than in the winter polar region, where the cooling is only about
957 8K. In the mesosphere, the cooling due to the direct forcing of CO_2 is even
958 stronger: 15 K.

959 The ozone concentration changes due to changes in the CO_2-concentration
960 as well as by changes in the SSTs. The temperature changes caused by this
961 change in ozone concentration generally mitigate the cooling caused by the
962 direct forcing of CO_2. However, in the tropical lower stratosphere and in some
963 regions of the mesosphere, the ozone feedback cools these regions further. In
964 the tropical lower stratosphere, for example, there is a cooling of 1K due to
965 the ozone feedback.
966
967 We also have seen that the global mean temperature response due to
968 dynamical feedbacks is small in the global average in all regions: less than 1
969 K. However, local responses to the changes in dynamics can be large.
970 Doubling the CO_2 leads to a stronger summer-to-winter-pole flow, which leads
971 to a cooling of the summer mesosphere and a warming of the winter
972 mesosphere. Changing the SSTs weakens this effect in the mesosphere, but
973 affects the temperature response in the stratosphere and lower mesosphere.
974
975 Using CFRAM on WACCM data shows that the change in water vapour leads
976 to a cooling of up to 2 K in the lower stratosphere. It should be noted that
977 climate models currently have a limited representation of the processes
978 determining the distribution and variability of lower stratospheric water vapour.
979 This means that the temperature response to the water vapour feedback
980 might be different using a different model. We have also seen a small effect of
981 the cloud and albedo feedback on the temperature response in the lower
982 stratosphere, while these feedbacks play no role in the upper stratosphere
983 and the mesosphere.
984

The results seen in this study are consistent with earlier findings. As in *Shepherd et al.*, (2008), we find that the higher the temperature at a region in the atmosphere, the more cooling there is seen due to the direct feedback of CO_2. We find, as in *Zhu et al.*, (2016) that the temperature responses due to the direct forcing of CO_2 follow the temperature distribution quite closely, while the temperature responses due to O_3 follow the changes in ozone concentration instead.

We have also seen that the ozone feedback generally yields a radiative feedback that mitigates the cooling, which is due to the direct forcing of CO_2, which is consistent with earlier studies such as *Jonsson et al., (2004), Dietmüller et al., (2014)*. CFRAM is the first study that allows for calculating how much of the temperature response is due to which feedback process.

The next step would be to investigate the exact mechanisms behind the feedback processes in more detail. Some processes can influence the different feedback processes, such as ozone depleting chemicals influencing the ozone concentration and thereby the temperature response of this feedback. A better understanding of the effect of the increased CO_2-concentration on the middle atmosphere, will help to distinguish the effects of the changes CO_2- and O_3-concentration.

There is also a need for a better understanding of how different feedbacks in the middle atmosphere affect the surface climate. As discussed in the introduction, the exact importance of ozone feedback on the global mean temperature is currently not clear (*Nowack et al.*, 2015, *Marsh et al.*, 2016). A similar analysis as in this paper can be performed to quantify the effects of feedbacks on the surface climate.

In conclusion, we have seen that CFRAM is an efficient method to quantify climate feedbacks in the middle atmosphere, although there is a relatively large error due to the linearization in the model. The CFRAM allows for separating and estimating the temperature responses due an external forcing and various climate feedbacks, such as ozone, water vapour, cloud, albedo and dynamical feedbacks. More research into the exact mechanisms of these feedbacks could help us to understand the temperature response of the middle atmosphere and their effects on the surface and tropospheric climate better.

Appendix: Formulation of CFRAM diagnostics using outputs of WACCM

The mathematical formulation of CFRAM is based on the conservation of total energy (*Lu and Cai*, 2009). At a given location in the atmosphere, the energy balance in an atmosphere-surface column can be written as:

$$\vec{R} = \vec{S} + \vec{Q}^{conv} + \vec{Q}^{turb} - \vec{D}^v - \vec{D}^h + \vec{W}^{fric} \qquad \text{(A1)}$$

$\vec{R}$ represents the vertical profile of the net long-wave radiation emitted by each layer in the atmosphere and by the surface. $\vec{S}$ is the vertical profile of the solar

1034   radiation absorbed by each layer. $\vec{Q}^{turb}$ is the convergence of total energy
1035   fluxes in each layer due to turbulent motions, $\vec{Q}^{conv}$ is convergence of total
1036   energy fluxes into the layers due to convective motion. $\vec{D}^{v}$ is the large-scale
1037   vertical transport of energy from different layers to others. $\vec{D}^{h}$ is the large-
1038   scale horizontal transport within the layers and $\vec{W}^{fric}$ is the work done by
1039   atmospheric friction. All terms in (A1) have units of Wm^{-2}.
1040
1041   Due to an external forcing (in this study, the change in CO_2-concentration
1042   and/or change in SSTs), the difference in the energy flux terms then
1043   becomes:
1044
1045 $\Delta\vec{R} = \Delta\vec{F}^{ext} + \Delta\vec{S} + \Delta\vec{Q}^{conv} + \Delta\vec{Q}^{turb} - \Delta\vec{D}^{v} - \Delta\vec{D}^{h} + \Delta\vec{W}^{fric}$ (A2)
1046
1047   In which the delta (Δ) stands for the difference between the perturbation run
1048   and the control run.
1049
1050   CFRAM takes advantage of the fact that the infrared radiation is directly
1051   related to the temperatures in the entire column. The temperature changes in
1052   the equilibrium response to perturbations in the energy flux terms can be
1053   calculated. This is done by requiring that the temperature-induced changes in
1054   infrared radiation balance the non-temperature induced energy flux
1055   perturbations.
1056
1057   Equation (A2) can also be written as:
1058
1059 $\Delta(\vec{S} - \vec{R})_{total} + \Delta dyn = 0$ (A3)
1060
1061   The term $\Delta(\vec{S} - \vec{R})$ can be calculated as the longwave heating rate and the
1062   solar heating rate are output variables of the model simulations. We take the
1063   time mean of the WACCM data and perform the calculations for each grid
1064   point of the WACCM data. This means that in the end, we will have the
1065   temperature changes at each latitude, longitude and height.
1066
1067   We then calculate the difference in these heating rates for the perturbation
1068   simulation and the control simulation.
1069
1070   We use the term $\Delta(\vec{S} - \vec{R})_{total}$ to calculate the dynamics term Δdyn.
1071
1072 $\Delta dyn = -\Delta(\vec{S} - \vec{R})_{total}$ (A4)
1073
1074   WACCM provides us with a heating rate in Ks^{-1}. For the CFRAM calculations,
1075   we need the energy flux in Wm^{-2}. We can calculate the energy flux by
1076   multiplying with the mass of different layers in the atmosphere and the specific
1077   heat capacity.
1078
1079 $\Delta(\vec{S} - \vec{R}) = \Delta(\vec{S} - \vec{R})_{(WACCM)} * mass_k * c_p$ (A5)
1080

1081   In which $\Delta(\vec{S} - \vec{R})$ is the difference in the shortwave radiation $\vec{(S)}$ and
1082   longwave radiation $\overrightarrow{(R)}$) between the perturbation run and the control run as a
1083   flux in Wm⁻², while $\Delta(\vec{S} - \vec{R})_{(WACCM)}$ is this difference as heating rate in Ks⁻¹ in
1084   WACCM, with $mass_k = \frac{p_{k+1} - p_k}{g}$ with p in Pa, $c_p = 1004$ $J\,kg^{-1}\,K^{-1}$ the
1085   specific heat capacity at constant pressure and *g* the gravitational
1086   acceleration 9.81 *ms⁻²*.
1087
1088   WACCM includes a non-local thermal equilibrium (non-LTE) radiation scheme
1089   above 50 km. It consists of a long-wave radiation (LW) part and a short-wave
1090   radiation (SW) part which includes the extreme ultraviolet (EUV) heating rate,
1091   chemical potential heating rate, CO_2 near-infrared (NIR) heating rate, total
1092   auroral heating rate and non-EUV photolysis heating rate.
1093   Therefore, we split the term $\Delta(\vec{S} - \vec{R})_{total}$ in an LTE and a non-LTE term:
1094
1095 $\Delta(\vec{S} - \vec{R})_{total} = \Delta(\vec{S} - \vec{R})_{LTE} + \Delta(\vec{S} - \vec{R})_{non-LTE}$ (A6)
1096
1097   WACCM provides us with the total longwave heating rate as well as the total
1098   solar heating rate and the non-LTE longwave and shortwave heating rates for
1099   the different runs. This means that we can calculate the term $\Delta(\vec{S} - \vec{R})_{non-LTE}$
1100   as well, where we again need to convert our result from Ks⁻¹ to Wm⁻²:
1101
1102 $\Delta(\vec{S} - \vec{R})_{non-LTE} = \Delta(\vec{S} - \vec{R})_{non-LTE(WACCM)} \; mass_k * c_p$ (A7)
1103
1104   This term can be inserted in equation (3):
1105
1106 $\Delta(\vec{S} - \vec{R})_{LTE} + \Delta(\vec{S} - \vec{R})_{non-LTE} + \Delta dyn = 0$ (A8)
1107
1108   The central step in CFRAM is to decompose the radiative flux vector, using a
1109   linear approximation.
1110
1111   We start by decomposing the LTE infrared radiative flux vector $\Delta\vec{R}$
1112
1113 $\Delta\vec{R}_{LTE} = \frac{\partial\vec{R}}{\partial\vec{T}}\Delta T + \Delta\vec{R}_{CO_2} + \Delta\vec{R}_{O_3} + \Delta\vec{R}_{H_2O} + \Delta\vec{R}_{albedo} + \Delta\vec{R}_{cloud}$ (A9)
1114
1115   where $\Delta\vec{R}_{CO_2}$, $\Delta\vec{R}_{O_3}$, $\Delta\vec{R}_{H_2O}$, $\Delta\vec{R}_{albedo}$, $\Delta\vec{R}_{cloud}$ are the changes in infrared
1116   radiative fluxes due to the changes in CO_2, ozone, water vapour, albedo and
1117   clouds, respectively.
1118
1119   For equation (A9), we assumed that radiative perturbations can be linearized
1120   by neglecting the higher order terms of each thermodynamic feedback and
1121   the interactions between these feedbacks. This is also commonly done in the
1122   PRP method (*Bony et al.,* 2006).
1123
1124   The term $\frac{\partial\vec{R}}{\partial\vec{T}}\Delta T$ represents the changes in the IR radiative fluxes related to the
1125   temperature changes in the entire atmosphere-surface column. The matrix $\frac{\partial\vec{R}}{\partial\vec{T}}$

1126 is the Planck feedback matrix, in which the vertical profiles of the changes in
1127 the divergence of radiative energy fluxes due to a temperature change are
1128 represented.

1130 We calculate this feedback matrix using the output variables of the
1131 perturbation and the control run of WACCM and inserting these in the CFRAM
1132 radiation code: atmospheric temperature, surface temperature, reference
1133 height temperature, ozone, surface pressure, solar insolation, downwelling
1134 solar flux at the surface, net solar flux at the surface, dew point temperature,
1135 cloud fraction, cloud ice amount, cloud liquid amount, ozone and specific
1136 humidity.

1138 Similarly, the changes in the LTE shortwave radiation flux can be written as
1139 the sum of the change in shortwave radiation flux due to the direct forcing of
1140 CO_2 and the different feedbacks:

1142 $$\Delta \vec{S}_{LTE} = \Delta \vec{S}_{CO_2} + \Delta \vec{S}_{O_3} + \Delta \vec{S}_{H_2O} + \Delta \vec{S}_{albedo} + \Delta \vec{S}_{cloud} \qquad \text{(A10)}$$

1144 Similarly, to equation (A9), we perform a linearization.

1146 Substituting (A9) and (A10) in equation (A8) yields:

1148 $$\Delta(\vec{S}-\vec{R})_{CO_2} + \Delta(\vec{S}-\vec{R})_{O_3} + \Delta(\vec{S}-\vec{R})_{H_2O} + \Delta(\vec{S}-\vec{R})_{albedo} + \Delta(\vec{S}-\vec{R})_{cloud} - \frac{\partial \vec{R}}{\partial \vec{T}}\Delta T$$
1149 $$+\Delta(\vec{S}-\vec{R})_{non-LTE} + \Delta dyn = 0 \qquad \text{(A11)}$$

1151 This can be written as:

1153 $$\Delta T = \left(\frac{\partial \vec{R}}{\partial \vec{T}}\right)^{-1} \Big\{ \Delta(\vec{S}-\vec{R})_{CO_2} + \Delta(\vec{S}-\vec{R})_{O_3} + \Delta(\vec{S}-\vec{R})_{H_2O} + \Delta(\vec{S}-\vec{R})_{albedo} +$$
1154 $$\Delta(\vec{S}-\vec{R})_{cloud} + \Delta(\vec{S}-\vec{R})_{non-LTE} + \Delta dyn \Big\} \qquad \text{(A12)}$$

1157 **Acknowledgements**

1159 The computations and simulations were performed on resources provided by
1160 the Swedish National Infrastructure for Computing (SNIC) at National
1161 Supercomputer Center (NSC) in Linköping.

1163 Hamish Struthers NSC is acknowledged for assistance concerning technical
1164 aspects in making the WACCM code run on NSC supercomputer Tetralith.
1165 We thank Qiang Zhang for helping to make the radiation model code
1166 applicable to WACCM model data.

1168 **Competing interests**

1170 The authors have no competing interests to declare.

1172 **References**

1173

1174 Akmaev, R.A., Fomichev, V.I. and Zhu, X.: Impact of middle-
1175 atmospheric composition changes on greenhouse cooling in the upper
1176 atmosphere, *Journal of Atmospheric and Solar-Terrestrial Physics*, 68, 1879-
1177 1889, doi:10.1016/j.jastp.2006.03.008, 2006.

1178

1179 Beig, G., et al.: Review of mesospheric temperature trends, *Reviews of*
1180 *Geophysics,* 41(4), doi:10.1029/2002RG000121, 2003.

1181

1182 Bony, S., and co-authors: How well do we understand and evaluate climate
1183 change feedback processes?, *Journal of Climate*, 19(15), 3445–3482,
1184 doi:10.1175/JCLI3819.1, 2006.

1185

1186 Boucher, O., Randall, D., and co-authors: Clouds and Aerosols, in: *Climate*
1187 *Change: The Physical Science Basis. Contribution of Working Group I to*
1188 *IPCC AR5*, edited by: Stocker T.F. and coauthors., Cambridge University
1189 Press, Cambridge, United Kingdom and New York, NY, USA, 2013.

1190 Brasseur, G. P., and Solomon, S.: Aeronomy of the middle atmosphere,
1191 Chemistry and physics of the stratosphere, Springer, New York, 2005.

1192 Brewer, A. W.: Evidence for a world circulation provided by the measurements
1193 of helium and water vapour distribution in the stratosphere. *Quarterly Journal*
1194 *of the Royal Meteorological Society*, 75(326), 351-363,
1195 doi:10.1002/qj.49707532603, 1949.

1196

1197 Brühl, C., & Crutzen, P. J.: Scenarios of possible changes in atmospheric
1198 temperatures and ozone concentrations due to man's activities, estimated
1199 with a one-dimensional coupled photochemical climate model, *Climate*
1200 *Dynamics*, 2(3), 173-203, doi: /10.1007/BF01053474, 1988.

1201 Butchart, N., and co-authors: Chemistry–climate model simulations of twenty-
1202 first century stratospheric climate and circulation changes, *Journal of Climate*,
1203 23(20), 5349–5374, doi:10.1175/2010JCLI3404.1, 2010.

1204 Caldwell, P.M., Zelinka, M.D., Taylor, K.E., Marvel, K.: Quantifying the
1205 sources of intermodal spread in equilibrium climate sensitivity, *Journal of*
1206 *Climate*, 29, 513-524, doi:10.1175/JCLI-D-15-0352.1, 2016.

1207

1208 Cai, M., and Lu, J.: A new framework for isolating individual feedback
1209 processes in coupled general circulation climate models. Part II: Method
1210 demonstrations and comparisons, *Climate dynamics*, 32(6), 887-900,
1211 doi:10.1007/s00382-008-0424-4, 2009.

1212

1213 Cariolle, D.: The ozone budget in the stratosphere: Results of a one-
1214 dimensional photochemical model, *Planetary and Space Science*, 31(9),
1215 1033-1052, doi:10.1016/0032-0633(83)90093-4, 1983.

1216

1217 Deckert, R. and Dameris, M.: Higher tropical SSTs strengthen the tropical
1218 upwelling via deep convection, *Geophysical Research Letters*, *35*(10), doi:
1219 10.1029/2008GL033719, 2008.

1221 Dobson, G. M. B.: Origin and distribution of the polyatomic molecules in the
1222 atmosphere. *Proceedings of the Royal Society of London. Series A.*
1223 *Mathematical and Physical Sciences*, *236*(1205), 187-193,
1224 doi:10.1098/rspa.1956.0127, 1956.

1226 Fomichev, V.I., Jonsson, A.I., De Grandpre, J., Beagley, S.R., McLandress,
1227 C., Semeniuk, K., Shepherd, T.G.: Response of the middle atmosphere to
1228 CO_2 doubling: Results from the Canadian Middle Atmosphere Model*, Journal*
1229 *of Climate*, 20(7), 1121-1141, doi:10.1175/JCLI4030.1, 2007.

1231 Fu, Q., and Liou, K. N.: On the correlated k-distribution method for radiative
1232 transfer in nonhomogeneous atmospheres. *Journal of the Atmospheric*
1233 *Sciences*, *49*(22), 2139-2156, doi:10.1175/1520-
1234 0469(1992)049<2139:OTCDMF>2.0.CO;2, 1992.

1236 Fu, Q., and Liou, K. N.: Parameterization of the radiative properties of cirrus
1237 clouds. *Journal of the Atmospheric Sciences*, *50*(13), 2008-2025, doi:
1238 10.1175/1520-0469(1993)050<2008:POTRPO>2.0.CO;2 1993.

1240 Hu, X., Y. Li, S. Yang, Y. Deng and Cai. M.: Process-based decomposition of
1241 the decadal climate difference between 2002-13 and 1984-95, J. Climate, 30,
1242 4373–4393, doi: 10.1175/JCLI-D-15-0742.1, 2017.

1244 Hurrell, J.W., et al.: The Community Earth System Model: A framework for
1245 collaborative research. *Bulletin of the American Meteorological Society*, *94*(9),
1246 1339-1360, doi: 10.1175/BAMS-D-12-00121.1, 2013.

1247 Jaiser, R., K. Dethloff and Handorf, D.: Stratospheric response to Arctic sea
1248 ice retreat and associated planetary wave propagation changes, *Tellus A:*
1249 *Dynamic Meteorology and Oceanography*, 65(1), 19375, doi:
1250 10.3402/tellusa.v65i0.19375, 2013.

1251 Jonsson, A.I., de Grandpré, J., Fomichev, V.I., McConnell, J.C., Beagley,
1252 S.C.: Doubled CO_2-induced cooling in the middle atmosphere: Photochemical
1253 analysis of the ozone radiative feedback, *Journal of Geophysical Research*,
1254 109, D24103, doi:10.1029/2004JD005093, 2004

1255 Kinnison, D.E., Brasseur, G.P., Walters, S., Garcia, R.R. Marsh, D.R, Sassi,
1256 F., Harvey, V.L., Randall, C.E., Emmons, L., Lamarque, J.F., Hess, P.,
1257 Orlando, J.J., Tie, X.X., Randall, W., Pan, L.L., Gettelman, A., Granier, C.,
1258 Diehl, T., Niemeijer, Y., Simmons, A.J.: Sensitivity of chemical tracers to
1259 meteorological parameters in the MOZART–3 chemical transport model,
1260 *Journal of Geophysical Research: Atmospheres*, 112, D20302,
1261 doi:10.1029/2006JD007879, 2007.

1263 Langematz, U.: Stratospheric ozone: down and up through the
1264 anthropocene, *ChemTexts* 5, 8, doi/10.1007/s40828-019-0082-7, 2019.

1265 Lindzen, R.S.: Turbulence stress owing to gravity wave and tidal breakdown,
1266 *Journal of Geophysical Research: Oceans*, 86.C10, 9707–9714,
1267 doi:10.1029/JC086iC10p09707, 1981.

1268
1269 Lu, J., and Cai, M.: A new framework for isolating individual feedback
1270 processes in coupled general circulation climate model. Part I: Formulation.
1271 *Climate dynamics*, 32 (6), 873–885, doi:10.1007/s00382-008-0425-3, 2009.
1272
1273 Manabe, S., & Wetherald, R. T.: The effects of doubling the CO_2
1274 concentration on the climate of a general circulation model. *Journal of the*
1275 *Atmospheric Sciences*, *32*(1), 3-15, 1975.

1276 Marsh, D.R., Mills, M.J. Kinnison, D.E., Lamarque, J.F., Calvo, N., Polvani,
1277 L.M.: Climate change from 1850 to 2005 simulated in CESM1(WACCM),
1278 *Journal of Climate*, 26, 7372–7391, doi:10.1175/JCLI-D-12-00558.1, 2013.

1279 Marsh, D.R., Lamarque, J.-F., Conley, A.J. and Polvani, L.M., Stratospheric
1280 ozone chemistry feedbacks are not critical for the determination of climate
1281 sensitivity in CESM1(WACCM), *Geophysical Research Letters*, 43, 3928–
1282 3934, doi:10.1002/2016GL068344, 2016.

1283 McFarlane, N.A., The effect of orographically excited wave drag on the
1284 general circulation of the lower stratosphere and troposphere, *Journal of*
1285 *Atmospheric Sciences,* 44(14), 1775–1800,
1286 doi:10.1175/15200469(1987)044<1775:TEOOEG>2.0.CO;2, 1987.

1287 Neale, R., Richter, J., Park, S., Lauritzen, P., Vavrus, S., Rasch, P. and
1288 Zhang, M: The mean climate of the Community Atmosphere Model (CAM4) in
1289 forced SST and fully coupled experiments, *Journal of Climate*, 26, 5150–
1290 5168, doi:10.1175/JCLI- D-12-00236.1, 2013.

1291 Nowack, P.J., Abraham, N.L., Maycock, A.C., Braesicke, P., Gregory, J.M.,
1292 Joshi, M.M., Osprey, A., Pyle, J.A.: A large ozone-circulation feedback and its
1293 implications for global warming assessments, *Nature Climate Change*, 5 (1),
1294 41-45, 2015, doi:10.1038/NCLIMATE2451, 2015.

1295 Oberländer, S., Langematz, U. and Meul, S.: Unraveling impact factors for
1296 future changes in the Brewer-Dobson circulation, *Journal of Geophysical*
1297 *Research: Atmospheres*, 118, 10296-10312, doi:10.1002/jgrd.50775, 2013.
1298
1299 Ramaswamy, V., Collins, W., Haywood, J., Lean, J., Mahowald, N., Myhre,
1300 G., Naik, V., Shine, K.P., Soden, B., Stenchikov, G., Storelvmo, T., 2019:
1301 Radiative forcing of climate: The historical evolution of the radiative forcing
1302 concept, the forcing agents and their quantification, and application,
1303 *Meteorological Monographs* 59, 14.1 14.99,
1304 doi:10.1175/AMSMONOGRAPHS-D-19-0001.1

1305
1306 Ramaswamy, V., et al.: Stratospheric temperature trends: Observations and
1307 model simulations, *Reviews of Geophysics* 39.1, 71-122, doi:
1308 10.1029/1999RG000065, 2001.
1309
1310 Richter, J.H., Sassi, F., Garcia, R.R.: Toward a physically based gravity wave
1311 source parameterization in a general circulation model, *Journal of the*
1312 *Atmospheric Sciences*, 67, 136–156, doi:10.1175/2009JAS3112.1, 2010.
1313 Rieger, V.S., Dietmüller, S., Ponater, M.: Can feedback analysis be used to
1314 uncover the physical origin of climate sensitivity and efficacy differences?,
1315 *Climate Dynamics* 49, 2831-2844, doi: 10.1007/s00382-016-3476-x 2017.
1316 Riese, M., Ploeger, F., Rap, A., Vogel, B., Konopka, P., Dameris, M., &
1317 Forster, P.: Impact of uncertainties in atmospheric mixing on simulated UTLS
1318 composition and related radiative effects, *Journal of Geophysical Research:*
1319 *Atmospheres*, *117*(D16), doi:10.1029/2012JD017751, 2012.
1320
1321 Royer, J.F., Planton, S., Déqué, M.: A sensitivity experiment for the removal
1322 of Arctic sea ice with the French spectral general circulation model, *Climate*
1323 *Dynamics*, 5(1), 1-17, doi:10.1007/BF00195850, 1990.
1324
1325 Schmidt, H., Brasseur, G.P, Charron, M., Manzini, E., Giorgetta, M.A., Diehl,
1326 T., Fomichev, V., Kinnison, D., Marsh, D., Walters, S., The HAMMONIA
1327 Chemistry Climate Model: Sensitivity of the mesopause region to the 11-year
1328 solar cycle and CO_2 doubling, *Journal of Climate,* 19(16), 3903-3931,
1329 doi:10.1175/JCLI3829.1, 2006.
1330
1331 Shaw, T.A., and Shepherd T.G.: Atmospheric science: Raising the
1332 roof, *Nature geoscience,* 1(1), 12, doi:10.1038/ngeo.2007.53, 2008.
1333 Shepherd, T.G.: Dynamics, stratospheric ozone and climate change,
1334 *Atmosphere-Ocean*, 46,1, 117-138, doi:10.3137/ao.460106, 2008.
1335 Shepherd, T.G., and McLandress, C.: A robust mechanism for strengthening
1336 of the Brewer–Dobson circulation in response to climate change: critical layer
1337 control of subtropical wave breaking, *Journal of the Atmospheric Sciences*,
1338 68, 4, 784-797, doi:10.1175/2010JAS3608, 2011.
1339 Shine, K. P., et al.: A comparison of model-simulated trends in stratospheric
1340 temperatures, *Quarterly Journal of the Royal Meteorological Society: A journal*
1341 *of the atmospheric sciences, applied meteorology and physical*
1342 *oceanography* 129(590),1565-1588, doi:10.1256/qj.02.186, 2003.
1343
1344 Sigmond, M., Siegmund, P.C., Manzini, E. and Kelder, H.: A simulation of the
1345 separate climate effects of middle-atmospheric and tropospheric CO_2
1346 doubling, *Journal of Climate*, 17(12), 2352-2367, doi:10.1175/1520-
1347 0442(2004)017<2352:ASOTSC>2.0.CO;2, 2004.

1348 Soden, B., Held, I.M.,: An assessment of climate feedbacks in coupled ocean-
1349 atmosphere models, *Journal of Climate*, 19, 3354-3360,
1350 doi:10.1175/JCLI3799.1, 2006.

1351 Solomon, S., Rosenlof, K. H., Portmann, R. W., Daniel, J. S., Davis, S. M.,
1352 Sanford, T. J., & Plattner, G. K.: Contributions of stratospheric water vapor to
1353 decadal changes in the rate of global warming, *Science*, *327*(5970), 1219-
1354 1223, doi: 10.1126/science.1182488, 2010.
1355
1356 Song, X., and Zhang, G.J.: Role of climate feedback in El Niño-like SST
1357 response to global warming, *Journal of Climate*, 27, 7301–7318,
1358 doi:10.1175/JCLI-D-14-00072.1, 2014
1359
1360 Taylor, P.C., Cai, M., Hu, A., Meehl, J., Washington, W. and Zhang, G.J.: A
1361 decomposition of feedback contributions to polar warming amplification,
1362 *Journal of Climate*, 26, 7023–7043, doi:10.1175/JCLI-D-12-00696.1, 2013.
1363
1364 WMO (World Meteorological Organization), *Scientific Assessment of Ozone*
1365 *Depletion: 2018*, Global Ozone Research and Monitoring Project – Report No.
1366 58, 588 pp., Geneva, Switzerland, 2018.
1367
1368 Zhang, P., Wu, Y., Simpson, I.R., Smith, K.L., Zhang, X., De, B., and
1369 Callaghan, P.: A stratospheric pathway linking a colder Siberia to Barents-
1370 Kara Sea sea ice loss, *Science Advances*, 4(7), eaat6025, doi:
1371 10.1126/sciadv.aat6025, 2018.
1372
1373 Zheng, J., Zhang, Q., Li, Q., Zhang, Q. and Cai, M., Contribution of sea ice
1374 albedo and insulation effects to Arctic amplification in the EC-Earth Pliocene
1375 simulation*, Climate of the Past*, 15, 291-305, doi:10.5194/cp-15-291-2019,
1376 2019.
1377
1378 Zhu, X., Yee, J.-H., Cai, M., Swartz, W.H., Coy, L., Aquila, V., Garcia, R.,
1379 Talaat, E.R.: Diagnosis of middle-atmosphere climate sensitivity by the
1380 climate feedback-response analysis method, *Journal of Atmospheric*
1381 *Sciences*, 73(1), 3-23, doi:10.1175/JAS-D-15-0013.1, 2016.